

## Characterizations of Aircraft Icing Environments that Include Supercooled Large Drops

STEWART G. COBER, GEORGE A. ISAAC, AND J. WALTER STRAPP

*Cloud Physics Research Division, Meteorological Service of Canada, Downsview, Ontario, Canada*

(Manuscript received 13 November 2000, in final form 20 April 2001)

### ABSTRACT

Measurements of aircraft icing environments that include supercooled large drops (SLD) greater than  $50\ \mu\text{m}$  in diameter have been made during 38 research flights. These flights were conducted during the First and Third Canadian Freezing Drizzle Experiments. A primary objective of each project was the collection of in situ microphysics data in order to characterize aircraft icing environments associated with SLD. In total there were 2793 30-s averages obtained in clouds with temperatures less than or equal to  $0^\circ\text{C}$ , maximum droplet sizes greater than or equal to  $50\ \mu\text{m}$ , and ice crystal concentrations less than  $1\ \text{L}^{-1}$ . The data include measurements from 12 distinct environments in which SLD were formed through melting of ice crystals followed by supercooling in a lower cold layer and from 27 distinct environments in which SLD were formed through a condensation and collision-coalescence process. The majority of the data were collected at temperatures between  $0^\circ$  and  $-14^\circ\text{C}$ , in stratiform winter clouds associated with warm-frontal or low pressure regions. For in-cloud measurements with temperatures less than or equal to  $0^\circ\text{C}$ , the relative fraction of liquid-, mixed-, and glaciated-phase conditions were 0.4, 0.4, and 0.2, respectively. For each 30-s (3 km) measurement, integrated drop spectra that spanned  $1\text{--}3000\ \mu\text{m}$  were determined using measurements from forward-scattering spectrometer probes and 2D-C and 2D-P probes. The integrated liquid water content (LWC) for each drop spectrum was compared with the LWC measured with a Nevzorov total water content probe and a Rosemount icing detector. The agreement was within the errors expected for such comparisons. This provides confidence in the droplet spectra measurements, particularly in the assessment of extreme conditions. The 99.9th-percentile LWC value was  $0.7\ \text{g m}^{-3}$ , and the 99th-percentile LWC for drops greater than  $50\ \mu\text{m}$  in diameter was  $0.2\ \text{g m}^{-3}$ . The 99.5th-percentile values of LWC and droplet concentrations are determined for different horizontal length scales and droplet diameter intervals, and are used to characterize the extreme icing conditions observed. The largest median volume diameters (MVD) observed were approximately  $1000\ \mu\text{m}$  and represent cases in which the aircraft was flown below cloud base in freezing-rain conditions. In one case, SLD was observed to form at  $-21^\circ\text{C}$ , and the associated icing was rated as severe. Approximately 3% of the data for which SLD were observed had LWC greater than  $0.2\ \text{g m}^{-3}$  and MVD greater than  $30\ \mu\text{m}$ . Such conditions are believed to represent conditions that have the largest potential effects on aircraft performance. The analysis is presented in a format that is suitable for several applications within the aviation community, and comparisons are made to four common icing-envelope formulations. The data should be beneficial to regulatory authorities who are currently attempting to assess certification requirements for aircraft that are expected to encounter freezing-precipitation conditions.

### 1. Introduction

There have been several reported in situ measurements of aircraft icing environments associated with freezing precipitation, including Sand et al. (1984), Cooper et al. (1984), Politovich (1989), Pobanz et al. (1994), Cober et al. (1996), Ashenden and Marwitz (1998), and Miller et al. (1998). These conditions have been variously referred to as freezing drizzle, freezing rain, supercooled large drops (SLD) and supercooled drizzle drops. Most of these observations were isolated and inadvertent, being made during research flights that had

other scientific objectives. Regardless, several of these reports have included comments about the apparent severity of the encounter with respect to the effects on the research aircraft, for example an unusual loss of aircraft performance such as reduction in climb rate or increase in drag, or an unusually fast buildup of ice on the windows, wings, or instruments. Attention toward the aircraft hazard associated with this phenomenon has been particularly strong following the crash of an ATR-72 commuter aircraft near Roselawn, Indiana, in October of 1994. It is believed that a primary factor in the accident was the accumulation of ice behind the aircraft's deicing boots and that this icing was associated with supercooled drizzle drops (Marwitz et al. 1997).

Whereas the explanation of the ATR-72 accident was somewhat speculative, hazards associated with freezing precipitation have been documented. Lewis (1951) dis-

---

*Corresponding author address:* Stewart Cober, Cloud Physics Research Division, Meteorological Service of Canada, 4905 Dufferin Street, Downsview, ON M3H 5T4, Canada.  
E-mail: stewart.cober@ec.gc.ca

cussed the high collision efficiencies and irregular ice formations associated with freezing drizzle and freezing rain. Sand et al. (1984) discussed two cases in which their King-Air research aircraft was diverted out of an icing region because the pilot assessed that the conditions were unusually hazardous. The pilot's assessments were partly based on an unusually rapid reduction in the cruising speed of the aircraft. Both cases occurred in the presence of SLD up to  $300 \mu\text{m}$  in diameter, and both cases had ice accumulation under the wings in unprotected areas. Cober et al. (1996) described how a Convair-580 research aircraft was diverted out of a freezing-drizzle region after 2 min of exposure. The pilot's decision to divert was based on an unusually rapid rate of ice accumulation on the pilot windows. The cloud environment had drops to  $500 \mu\text{m}$  at  $-7.5^\circ\text{C}$ , with a liquid water content (LWC) of less than  $0.1 \text{ g m}^{-3}$ . Politovich (1996) showed that the largest changes to aircraft performance occurred in clouds with LWC greater than  $0.2 \text{ g m}^{-3}$  and droplet median volume diameter (MVD) greater than  $30 \mu\text{m}$ . Ashenden and Marwitz (1998) characterized the response of a turboprop aircraft in several SLD conditions and suggested that drizzle-sized drops caused the largest potential hazard. Bernstein et al. (1999) described a situation in which the National Aeronautics and Space Administration Glenn Research Center Twin Otter was flown in a freezing-rain region and concluded that freezing-rain conditions can present a significant hazard to aircraft. Helicopter pilots have reported cases in which freezing drizzle below the bases of stratiform clouds caused severe icing on their aircraft (Fuchs and Schickel 1995).

Characterizing the aircraft icing environments associated with freezing precipitation is an important research objective for the U.S. Federal Aviation Administration (FAA) and Transport Canada. The 1997 FAA Inflight Aircraft Icing Plan contains explicit requirements to consider a comprehensive redefinition of the current aircraft icing certification envelopes when sufficient information is available worldwide on SLD, mixed-phase conditions, and other icing conditions. Differences in instrumentation, analysis techniques, and reporting procedures have made it difficult to combine the isolated measurements of SLD conditions into a consistent database, which might be used to characterize the aircraft icing environments associated with freezing precipitation. In addition, the collective dataset is unlikely to be large enough to allow an accurate statistical analysis of extreme conditions. As a consequence, several field projects have recently been conducted to attempt to fulfill this aim (Isaac et al. 1998; Miller et al. 1998). The results from two such field projects will be presented here.

In situ measurements of freezing-precipitation environments have several other important applications, including 1) to provide realistic hydrometeor spectra and environmental data for use in numerical icing simulation models (Boutanios et al. 1998), 2) to provide spectra

for comparison with spectra produced in icing wind tunnels (Miller et al. 1996; Ashenden et al. 1996) or behind aircraft icing tankers (Ashenden and Marwitz 1998), and 3) to provide sufficient data to develop microphysics parameterizations that could be used in icing forecast algorithms (e.g., Reisner et al. 1998; Tremblay and Glazer 2000).

## 2. The Canadian Freezing Drizzle Experiments

The First Canadian Freezing Drizzle Experiment (CFDE I) was conducted during 1–25 March 1995. It was based from St. John's, Newfoundland, and consisted of 12 research flights into winter storms for which freezing-precipitation conditions were forecast to exist. St. John's was chosen as the center for operations because it receives in excess of  $150 \text{ h yr}^{-1}$  of freezing precipitation (McKay and Thompson 1969; Stuart and Isaac 1999). The peak frequency occurs in February and March when an average of  $30 \text{ h month}^{-1}$  of freezing precipitation is observed at the surface. Strapp et al. (1996) correlated surface observations at St. John's with radiosonde measurements and showed that approximately 75% of the observations of freezing precipitation were associated with drizzle that formed through a condensation and collision-coalescence process (Singleton 1960; Bocchieri 1980; Huffman and Norman 1988; Beard and Ochs 1993), and 25% formed through a melting and resupercooling process (Stewart 1992; Stewart and Crawford 1995). These formation mechanisms are referred to here as nonclassical and classical, respectively.

CFDE I was designed subsequent to the Second Canadian Atlantic Storms Program (CASP II), which was conducted during the winter of 1992 (Stewart 1991). During CASP II, freezing-drizzle observations were made on four separate research flights (Cober et al. 1995). In two of the encounters, the ice buildup on the front pilot windows was sufficiently rapid that the pilot felt it necessary to divert the aircraft out of the icing region. In all four cases, the aircraft vertical sounding indicated that the drizzle had formed through a nonclassical mechanism. One of these cases is described in detail in Cober et al. (1996). The unexpected high frequency of these observations, combined with the realization that such conditions were reported to be particularly dangerous for aircraft (Sand et al. 1984; Politovich 1989), led to the proposal for CFDE I, in which flights specific to freezing precipitation research were anticipated. A primary research objective of CFDE I was to characterize the aircraft icing environments associated with freezing precipitation, with a view to providing measurements that could be used to help to redefine the current icing envelopes (see section 3). This was to be achieved by making extensive in situ microphysics measurements in regions where freezing precipitation was forming, with emphasis on regions in

which the nonclassical formation mechanism was predominant.

CFDE III was conducted between 11 December 1997 and 18 February 1998. The research aircraft was based out of Ottawa, and 26 flights were conducted into winter storms over southern Ontario, southern Quebec, Lake Ontario, and Lake Erie. The geographical region was selected for two reasons: 1) to obtain data in a continental region over which there was considerable air traffic, and 2) the region around Ottawa and Montreal has a high frequency of freezing precipitation with 50–75 h yr<sup>-1</sup> observed at the surface (Stuart and Isaac 1999). The research objectives were essentially the same as for CFDE I.

### 3. Icing envelopes

The FAA Regulation 25 Appendix C (FAR 25-C, Federal Aviation Administration 1999) provides a characterization of aircraft icing environments, with 99.9th-percentile curves (i.e., envelopes) that incorporate temperature, droplet mean effective diameter, and LWC. As discussed by Lewis (1951), mean effective diameter is approximately equal to the median volume diameter. MVD is more commonly used to characterize icing environments. Continuous maximum conditions are defined in FAR 25-C as representing extreme icing environments with a horizontal distance of approximately 33 km. Aircraft that are certified for flight in icing conditions are expected to be able to fly in icing environments characterized by these curves. The FAR 25-C curves were based on in situ data collected in the 1940s (Jones and Lewis 1949; Lewis and Bergrun 1952), and only include MVD values up to 40  $\mu\text{m}$ , although Jones and Lewis (1949) suggested that extreme freezing-rain conditions could be represented by a droplet MVD of 1000  $\mu\text{m}$ , LWC of 0.15 g m<sup>-3</sup>, and a horizontal extent of more than 100 km. It is well recognized (Jeck 1996) that freezing-precipitation conditions can have MVD values outside of the FAR 25-C envelopes and that either the FAR 25-C curves require modification or another method is required for describing these icing environments.

Jeck (1996) suggested that cloud hydrometeor data could be classified into several bins with widths between 50 and 500  $\mu\text{m}$ . For a large dataset, percentiles of LWC and droplet concentration could be computed for each bin. Meteorological conditions such as temperature or altitude would be considered separately. This characterization would provide a simple reference for comparison with the drop spectra from wind tunnel, aircraft tanker, and icing simulation models. The FAR 25-C use of droplet MVD for characterizing icing environments has been criticized by Jeck (1996), Ashenden and Marwitz (1998), and others. For cases in which the majority of LWC is incorporated in droplets of less than 50  $\mu\text{m}$ , droplet distribution MVDs tend to show relatively little scatter between cases with and without drops greater

than 50  $\mu\text{m}$ . On the other hand, for cases in which the LWC in drops greater than 50  $\mu\text{m}$  is similar to the LWC in drops less than 50  $\mu\text{m}$ , the MVD is extremely sensitive to small changes in the droplet spectrum measurement. In these cases, the LWC is often observed to be incorporated primarily in drop sizes in the 10–30- and 100–400- $\mu\text{m}$  ranges, which can cause the MVD to vary from, for example, 30 to 200  $\mu\text{m}$  for a small change in the droplet spectra. Jeck's proposal to show explicitly the LWC in specific bins would avoid the problems inherent with using MVD.

Ashenden and Marwitz (1998) have suggested using the 80% mass diameter (80VD) for characterization, although their analysis was oriented toward aircraft performance characteristics. They demonstrated that their Super King-Air 200 suffered the largest performance degradations, in terms of rate of change in the drag coefficient and rate of climb, when the product of the 80VD and LWC was in the range of 10–100  $\mu\text{m g m}^{-3}$ . They also determined the number of encounters per hour for which they observed the SLD LWC to exceed thresholds of 0.05, 0.10, and 0.30 g m<sup>-3</sup>. They characterized the observed SLD conditions as a function of horizontal length.

Newton (1978) described icing accumulation envelopes, which represented the potential accumulations of ice on a 3-in. cylinder in g cm<sup>-2</sup> h<sup>-1</sup>. The potential accumulation would depend completely on the collision–collection efficiency of the hydrometeor spectra, which is a function of aircraft speed and droplet size. However, for drops greater than approximately 50  $\mu\text{m}$  in diameter the collision efficiency would be essentially 1, and there would be no way to distinguish the accumulation associated with 50- $\mu\text{m}$  drops from that of 500- or 1000- $\mu\text{m}$  drops. Such a distinction may be important, as shown by Ashenden et al. (1996), who noted that drizzle drops can form rougher accretions than larger drops (because of the respective freezing times), which, in turn, has a greater effect on the lift and drag coefficients of the wings. Comparisons of the CFDE I and III data will be made with each characterization technique.

### 4. Research aircraft and instrumentation

The research aircraft used during CFDE I and III was the National Research Council (NRC) Convair-580 aircraft, which was described in Cober et al. (1995) and Isaac et al. (1998). There were three independent hot-wire LWC measurements, including a Particle Measuring Systems, Inc., (PMS) King probe (King et al. 1978, 1985), and Sky Tech Research, Inc., Nevzorov LWC and total water content (TWC) probes (Korolev et al. 1998b). Intercomparisons between the King LWC and Nevzorov LWC and TWC measurements are given in Cober et al. (2001a). They showed that the LWC measurements agreed to within  $\pm 15\%$ , with no significant systematic biases for any instrument, when the droplet

distributions contained insignificant mass in drops greater than  $100\ \mu\text{m}$  in diameter. The King and Nevzorov LWC probes increasingly underestimate the LWC associated with drops greater than  $40\ \mu\text{m}$  (Biter et al. 1987; Strapp et al. 2000). However, the design of the Nevzorov TWC probe minimizes this effect (Korolev et al. 1998b). Therefore, the Nevzorov TWC probe was used as the primary LWC measurement, with the King and Nevzorov LWC probes used to confirm consistency. In mixed-phase clouds, the Nevzorov LWC and TWC measurements were used to determine the actual LWC following the technique outlined in Cober et al. (2001a).

The aerosol and cloud droplet spectra were measured with a PMS passive cavity aerosol spectrometer probe (PCASP) and two PMS forward-scattering spectrometer probes (FSSP). The FSSP ranges were normally  $3\text{--}45$  and  $5\text{--}95\ \mu\text{m}$ , respectively. Calibration of the FSSPs and analysis of FSSP data have been described in Cober et al. (1995, 2001a). The FSSP measurements of concentration and LWC were found to agree to within  $\pm 34\%$  and  $\pm 38\%$ , respectively. FSSP measurements can be contaminated when ice crystals are present (Gardiner and Hallett 1985), because ice crystals can be interpreted by the instrument as droplets. Cober et al. (2001a) found that FSSP spectra for sizes greater than approximately  $35\ \mu\text{m}$  in diameter were biased by ice crystals when the ice crystal concentration measured with the 2D probes exceeded  $1\ \text{L}^{-1}$ . This result has significant implications for assessing the hydrometeor spectra in mixed-phase conditions, which will be discussed in section 5.

The hydrometeor spectra greater than  $100\ \mu\text{m}$  were measured with three PMS 2D probes, including 2D-C monoscale  $25\text{--}800\ \mu\text{m}$ , 2D-C grayscale  $25\text{--}1600\ \mu\text{m}$ , and 2D-P monoscale  $200\text{--}6400\ \mu\text{m}$ . Measurements in the first four channels of each 2D-C instrument were discarded because of depth-of-field uncertainties associated with these channels (Joe and List 1987; Korolev et al. 1998a) and because of the significant sizing errors that occur in these channels (Korolev et al. 1991, 1998a). Strapp et al. (2001) showed that the net spectrum error for this 2D-C probe, expressed as a sizing error, could be expected to be less than  $\pm 10\%$  for drops greater than or equal to  $125\ \mu\text{m}$  in diameter.

The hydrometeor images obtained with the 2D probes were processed following the center-in technique of Heymsfield and Parrish (1978). The 2D-C gray data were analyzed using the 50% shadow level, which effectively made it equivalent to a 2D-C mono probe. Particle images were segregated into circles (drops) and noncircles (ice crystals) using diameter, area, perimeter, and symmetry algorithms described by Cober et al. (2001a). They showed that, in liquid-phase conditions at temperatures greater than  $0^\circ\text{C}$ , in excess of 85% of the particle images were assessed as circles and hence were interpreted correctly as drops. In glaciated-phase conditions, between 5% and 40% of the processed particle images were assessed as circles, which could be

incorrectly interpreted as drops. The relative fractions of circles and noncircles were strongly dependent on particle size, with particles less than or equal to 8 pixels in diameter having the largest potential errors. The larger a particle is, the higher the resolution of its shape is, and hence the higher the accuracy is in distinguishing circles from noncircles. In glaciated clouds, a particle size of 11 pixels was required before the average fraction of circular particles dropped below 0.2. This result also has significant implications for assessing hydrometeor spectra in mixed-phase conditions and will be discussed in section 5.

A Sensor Systems, Goodrich Corporation, Rosemount icing detector (RID) was installed on the Convair-580 for both CFDE projects. It was calibrated against the LWC probes by Cober et al. (2001b), and was shown to be capable of estimating LWC to within  $\pm 50\%$  when the LWC was below the Ludlam limit (Ludlam 1951; Baumgardner and Rodi 1989). It gave consistent results in freezing-precipitation conditions, implying that it could be used as an independent estimate of the LWC for cases with significant mass in drops greater than  $100\ \mu\text{m}$ .

## 5. Assessing drop spectra

The data from each flight were initially averaged in sequential 30-s intervals, corresponding to a horizontal length scale of  $2.9 \pm 0.3\ \text{km}$ , where the  $\pm$  value represents one standard deviation from the mean. For each interval, data from the FSSP and 2D probes were combined to produce a drop spectrum from  $3$  to  $3000\ \mu\text{m}$ . The midpoint diameters of each bin were used to interpolate the normalized droplet spectrum to  $1\text{-}\mu\text{m}$  resolution, from  $1\text{-}\mu\text{m}$  to the maximum drop diameter. The interpolation was based on a linear fit between logarithmic diameter and concentration pairs. For regions in which the  $3\text{--}45\text{-}$  and  $5\text{--}95\text{-}\mu\text{m}$  FSSP measurements overlapped, the  $3\text{--}45\text{-}\mu\text{m}$  data were used unless they were assessed to have been biased because of icing or fogging. The spectra were interpolated between the last FSSP channel ( $\leq 95\ \mu\text{m}$ ) and the first useful 2D-C channel ( $125\ \mu\text{m}$ ) and between the last useful 2D-C channel and the first useful 2D-P channel. The 30-s averaging scale was chosen because it represented a short averaging scale and a scale that generally allowed sufficient 2D measurements for statistical significance. FSSP and 2D channels were required to have 10 counts per 30-s interval before they were used in the analysis. When the number of 2D counts per bin fell below 10, bins were combined until 10 counts were obtained. The spectra were truncated when there were fewer than 10 counts in sizes larger than the last useful bin. The maximum droplet diameter  $D_{\text{max}}$  for each spectrum was assessed as the midpoint of the last useful bin. For each spectrum that was measured at a temperature less than or equal to  $0^\circ\text{C}$ , the drops larger than  $50\ \mu\text{m}$  in diameter will be collectively referred to as SLD.

Cober et al. (2001a) identified the phase for each 30-s interval as being liquid, mixed, or glaciated. Liquid-phase cases were identified using several criteria, including the fraction of processed 2D images ( $\geq 125 \mu\text{m}$ ) that were circular greater than 0.85, visual examination of the 2D imagery indicating no or very few ice particles, concentration of irregular (i.e., ice crystals) images less than  $0.1 \text{ L}^{-1}$  as measured with the 2D probes, agreement between the LWC instruments to within  $\pm 15\%$ , and agreement between the LWC and TWC measurements within  $\pm 15\%$  except in cases with significant mass in drops greater than  $100 \mu\text{m}$ . For liquid-phase conditions, the entire FSSP spectra, 2D-C spectra greater than or equal to  $125 \mu\text{m}$ , and 2D-P spectra greater than or equal to  $1000 \mu\text{m}$  were used to produce the integrated drop spectra.

Mixed-phase conditions were identified when the instruments collectively demonstrated all of the following characteristics: ratio of LWC to TWC between 0.25 and 1.0, fraction of circular 2D images greater than or equal to  $125 \mu\text{m}$  greater than 0.4, FSSP concentrations greater than  $15 \text{ cm}^{-3}$ , visual assessment that the 2D images contained ice crystals, and an RID response greater than  $2 \text{ mV s}^{-1}$  (for temperatures less than  $-4^\circ\text{C}$ ). For mixed-phase conditions with ice-crystal concentrations of  $1\text{--}5 \text{ L}^{-1}$ , the FSSP measurements were assessed to be contaminated by ice particles and hence to be unreliable for sizes greater than  $35 \mu\text{m}$  (Cober et al. 2001a). This observation was similar for both FSSP instruments, regardless of the measurement range. When the data were averaged over the collective CFDE dataset, the FSSP measurements in cloud conditions with ice-crystal concentration of  $1\text{--}5 \text{ L}^{-1}$  were found to have concentrations of particles greater than  $35 \mu\text{m}$  that were up to 10 times the concentrations for conditions with no ice crystals. The implication is that, for the CFDE dataset, FSSP measurements should not be used to infer droplet spectra for sizes greater than  $35 \mu\text{m}$ , whenever the ice crystal concentration exceeds  $1 \text{ L}^{-1}$ .

The identification of circular 2D images for particles greater than or equal to  $125 \mu\text{m}$  is also subject to error in mixed-phase conditions. Because the circular recognition algorithms identify between 5% and 40% of ice particles (in glaciated clouds) as circular, assessing whether a circular image is a drop or ice crystal in a mixed-phase cloud can be ambiguous. There are three techniques that might be used to minimize the errors associated with interpreting crystals as drops:

- 1) Because the relative fraction of ice crystals that are identified as circular images decreases with increasing particle size, increasing the minimum acceptable particle size would reduce the potential errors.
- 2) The average circular particle fraction associated with ice crystals could be subtracted from each spectrum measured. However, this is subjective because the average circular fraction is based on an average over

TABLE 1. Summary of in-cloud 30-s averages made during CFDE I and CFDE III. The data are segregated by phase, average temperature  $T_a$ , maximum droplet size observed  $D_{\text{max}}$ , and ice-crystal concentration  $C$ .

Conditions	Observations
Liquid phase with $T_a > 0^\circ\text{C}$	688
Liquid phase with $T_a \leq 0^\circ\text{C}$ and $D_{\text{max}} < 50 \mu\text{m}$	1309
Liquid phase with $T_a \leq 0^\circ\text{C}$ and $D_{\text{max}} \geq 50 \mu\text{m}$	1651
Mixed phase with $T_a > 0^\circ\text{C}$	50
Mixed phase with $T_a \leq 0^\circ\text{C}$ and $D_{\text{max}} < 50 \mu\text{m}$	536
Mixed phase with $T_a \leq 0^\circ\text{C}$ , $D_{\text{max}} \geq 50 \mu\text{m}$ , and $C < 1 \text{ L}^{-1}$	1142
Mixed phase with $T_a \leq 0^\circ\text{C}$ , $D_{\text{max}} \geq 50 \mu\text{m}$ , and $1 \leq C < 5 \text{ L}^{-1}$	723
Mixed phase with $T_a \leq 0^\circ\text{C}$ , $D_{\text{max}} \geq 50 \mu\text{m}$ , and $C \geq 5 \text{ L}^{-1}$	524
Glaciated phase	1509
Total	8132

a large dataset, whereas the scatter in individual observations might be considerable.

- 3) Only consider for analysis the mixed-phase cases with relatively low ice-crystal concentrations ( $C < 1 \text{ L}^{-1}$ ). Presumably, the number of ice crystals that are identified as circular will be negligible for these cases.

The mixed-phase conditions were segregated by ice crystal concentration  $C$  into  $C < 1 \text{ L}^{-1}$ ,  $1 \leq C < 5 \text{ L}^{-1}$ , and  $C \geq 5 \text{ L}^{-1}$ . The drop spectra for cases with  $C \geq 5 \text{ L}^{-1}$  were not analyzed for the reasons outlined above. The remaining cases were analyzed using the complete FSSP spectra and the 2D-C spectra for channels greater than or equal to 9 pixels ( $225 \mu\text{m}$ ). The mixed-phase data with  $1 \leq C < 5 \text{ L}^{-1}$  are not used in the final analysis because of the overestimate of LWC and concentrations for FSSP-measured particle sizes greater than  $35 \mu\text{m}$ . However, they were analyzed for comparison and to illustrate the magnitudes of the associated errors. At worst, these data represent overestimates of the LWC and MVD values for these cases.

In total, there were 8132 30-s in-cloud data points observed during CFDE I and CFDE III. These data represented 44% of the entire in-flight time of 154 h. A 30-s data point was assessed as being in cloud if the following conditions were met: the 30-s average TWC was greater than  $0.005 \text{ g m}^{-3}$  and more than 20% of the 1-s data had TWC greater than  $0.005 \text{ g m}^{-3}$ . The in-cloud data points are summarized in Table 1. There were 1651 and 2389 liquid- and mixed-phase cases, respectively, for which the average temperature  $T_a$  was less than or equal to  $0^\circ\text{C}$  and  $D_{\text{max}}$  was greater than or equal to  $50 \mu\text{m}$ . For the mixed-phase observations, there were 1142 cases with  $C < 1 \text{ L}^{-1}$  and 723 cases with  $1 \leq C < 5 \text{ L}^{-1}$ . To assess the data over longer length scales, the data were also averaged at 60, 120, and 300 s, representing horizontal length scales of approximately 6, 12, and 30 km, respectively. For each spectrum, the LWC and MVD were computed, as were

the total concentration and LWC for each bin defined by Jeck (1996). For each variable and averaging interval, and for the liquid- and mixed-phase cases with  $T_a \leq 0^\circ\text{C}$ ,  $D_{\text{max}} \geq 50 \mu\text{m}$ , and  $C < 1 \text{ L}^{-1}$ , the 90th, 95th, and 99th percentiles were computed to attempt to determine extreme SLD conditions. The results are presented in section 8.

## 6. Overview of SLD environments

Table 2 provides a summary of microphysical measurements for SLD environments made during CFDE I and III, and Table 3 contains a brief description of the meteorological conditions for each SLD environment. A distinct SLD environment was identified whenever the following conditions were met: SLD was greater than or equal to  $50 \mu\text{m}$ , minimum temperature was less than or equal to  $0^\circ\text{C}$ , number of 30-s observations with SLD was greater than or equal to 4, and the environment was distinct with respect to other SLD environments observed during the research flight. An SLD environment may contain data collected over several hours and may include data from multiple vertical and horizontal profiles in a region of interest. On the other hand, an environment may contain data from a single vertical profile, collected for example, when the aircraft was descending to land at Ottawa. Within a single research flight, two or more SLD environments were considered as distinct if their associated meteorological processes were clearly different or if they were observed in different geographical regions. On average, 30 min of SLD data were collected for each SLD environment. In general, sufficient vertical profiles were made with the aircraft so that the SLD formation mechanism could be accurately determined.

The majority of flights were directed into or toward warm-frontal or low pressure regions associated with midlatitude synoptic winter storms. The clouds observed were stratus or stratiform in nature, without significant convection. The majority of clouds associated with SLD environments were at altitudes of less than 3 km, although eight cases at greater than 3 km and one case at 6 km were observed. In total, there are 39 SLD environments summarized in Tables 2 and 3. Nonclassical formation mechanisms accounted for 70% of the SLD environments for both projects, and many of the nonclassical observations occurred in regions for which classical freezing precipitation was predicted. Nonclassical SLD were observed several times to originate in low stratus clouds at the base of the melting layer. The majority of classical SLD environments observed during CFDE III were made during the ice storm of 1998 (Isaac et al. 1998). The ratio of observations with nonclassical and classical formation mechanisms cannot be interpreted in a meaningful way because of biases inherent in the way in which flights were planned and conducted.

There are distinct differences in the microphysics measurements between SLD environments from CFDE

I and CFDE III. Table 4 summarizes the average LWC, temperature, droplet concentration, MVD, and mixed-phase conditions for the two projects, segregated by formation mechanism. The average values in Table 4 weight each SLD environment equally independent of the actual duration for which SLD was collected. The SLD environments in CFDE III had mean and maximum LWC values that were 30%–40% higher than those in CFDE I. In contrast, the mean CFDE-III SLD LWC was only 50% of the CFDE-I value for nonclassical SLD environments. CFDE-I clouds had substantially lower droplet concentrations and higher MVD, which are consistent with observations expected in maritime clouds. This result is also consistent with the higher SLD LWC values observed in the CFDE-I SLD environments. The average temperatures for CFDE-III SLD environments were  $2^\circ\text{C}$  colder for classical cases and  $4^\circ\text{C}$  colder for nonclassical cases when compared with the CFDE I observations. Mixed-phase conditions were substantially more frequent for the CFDE-III nonclassical cases, which may be related to the colder temperatures and possibly to the differences in the drop size distributions. The higher frequency of large drops in CFDE-I SLD environments may allow for a more effective ice multiplication mechanism (Hallett and Mossop 1974), which could lead to a faster glaciation process and a reduction in the frequency of mixed-phase conditions. The higher LWC values observed in CFDE-III environments may be indicative of stronger cloud forcing, which could presumably maintain mixed-phase conditions for a longer period of time. There may have generally been a greater number of active ice nuclei in the continental CFDE-III clouds, which would lead to a higher frequency of mixed-phase conditions. However, ice nuclei measurements were not made in either project, so it was not possible to test this hypothesis.

For each field project, the cloud microphysics were similar for classical and nonclassical SLD environments, with two differences. The temperatures for classical environments tended to be warmer, which was expected given that the majority of these measurements were made around the base of the melting layer and top of the lower cold layer. Altitude restrictions for the aircraft often prevented making measurements in the lower cold layer. The classical environments tended to have significantly larger MVD and  $D_{\text{max}}$  values, which was consistent with measuring rain-sized drops of greater than  $500 \mu\text{m}$  below the melting layer. Nonclassical environments rarely generated drops greater than  $500 \mu\text{m}$ .

## 7. Overview of microphysics conditions

Histograms of in-cloud temperature measurements observed during CFDE I and III are shown in Fig. 1. The three curves represent liquid phase (L); liquid and mixed phases (LM); and liquid, mixed, and glaciated phases (LMG). The majority of measurements were made at temperatures between  $1^\circ$  and  $-14^\circ\text{C}$ . There

TABLE 2. Summary of microphysics measurements made during CFDE I and CFDE III, for regions in which SLD were encountered. The data are based on the 30-s averages and include only cases in which SLD was observed. Dur gives the duration in minutes that SLD conditions were measured. Here FM is the formation mechanism, as classical (C) or nonclassical (NC). Variable  $P$  is the fraction of 30-s observations that were mixed phase. Here  $T_a$  and  $T_m$  are the mean and minimum temperatures, respectively, for the SLD regions. Variables  $A_b$  and  $A_c$  are the minimum and maximum altitudes, respectively, of cloud regions in which SLD was observed. Variable  $N_d$  is the mean PCASP concentration for aerosols 0.13–3  $\mu\text{m}$  in diameter. Variables  $N_d$  and  $N_{d,\text{max}}$  are the mean and maximum FSSP droplet concentrations. The mean and maximum LWC are LWC and LWC<sub>max</sub>, respectively. The median and maximum median volume diameters are MVD and MVD<sub>max</sub>, respectively. Dmax is the maximum drop size observed. The mean and maximum LWC incorporated in droplets  $> 50 \mu\text{m}$  are  $L > 50$  and  $L > 50_{\text{max}}$ , respectively.

Date	Time (UTC)	Dur (min)	FM	$P$	$T_a$ (°C)	$T_m$ (°C)	$A_b$ (km)	$A_c$ (km)	$N_d$ (cm <sup>-3</sup> )	$N_{d,\text{max}}$ (cm <sup>-3</sup> )	LWC (g m <sup>-3</sup> )	LWC <sub>max</sub> (g m <sup>-3</sup> )	MVD (μm)	MVD <sub>max</sub> (μm)	Dmax (μm)	$L > 50$ (g m <sup>-3</sup> )	$L > 50_{\text{max}}$ (g m <sup>-3</sup> )
CFDE-I SLD encounters																	
2 Mar	1741–1917	53	NC	0.00	-1.4	-3.2	0.2	1.0	38	96	0.15	0.28	30	50	212	0.02	0.08
3 Mar	1917–1943	20	C	0.13	-1.3	-6.6	0.3	2.2	77	102	0.07	0.26	104	521	1500	0.04	0.12
6 Mar	2043–2115	19	C	0.03	1.6	-2.4	0.3	1.9	67	119	0.16	0.45	19	1076	2000	0.03	0.17
7 Mar	1656–1907	64	NC	0.11	-1.6	-8.7	0.3	3.1	30	55	0.15	0.34	33	182	525	0.04	0.15
9 Mar	1652–1916	110	NC	0.05	-5.1	-11.5	0.1	2.7	94	83	0.18	0.50	29	353	612	0.06	0.27
10 Mar	1557–1746	62	C	0.36	-1.2	-4.2	0.3	1.5	36	11	0.09	0.28	155	840	1900	0.09	0.19
10 Mar	1900–1904	4	NC	0.00	0.5	-2.3	2.1	3.3	45	9	0.12	0.23	41	50	200	0.03	0.07
14 Mar	1625–1802	35	NC	0.00	0.8	-0.9	0.1	2.0	50	12	0.07	0.19	62	176	425	0.03	0.09
14 Mar	1803–1830	18	C	0.03	1.2	-0.4	0.2	2.6	48	54	0.13	0.23	29	201	1600	0.05	0.16
14 Mar	1831–1855	11	NC	0.00	1.5	-1.2	0.4	1.8	35	11	0.08	0.23	41	163	287	0.03	0.11
15 Mar	1857–2034	28	NC	0.07	-3.9	-8.3	0.2	4.0	324	94	0.17	0.44	24	197	425	0.03	0.18
17 Mar	1538–1854	56	NC	0.14	-5.1	-6.8	0.6	1.3	86	95	0.19	0.36	20	38	312	0.00	0.07
18 Mar	1607–1758	18	C	0.03	1.9	-0.8	0.2	0.9	57	47	0.13	0.27	25	962	2000	0.04	0.09
18 Mar	1842–1846	3	NC	0.83	-7.0	-7.1	2.1	2.2	24	8	0.09	0.15	31	39	262	0.00	0.03
22 Mar	1450–1519	13	NC	0.92	-2.7	-4.4	2.2	2.7	378	79	0.24	0.51	25	86	412	0.07	0.27
22 Mar	1706–1708	2	NC	0.20	-8.2	-8.6	1.3	1.4	247	90	0.10	0.13	25	27	56	0.00	0.00
CFDE-III SLD encounters																	
11 Dec	2151–2336	37	NC	0.33	-4.6	-9.5	0.5	2.0	728	248	0.20	0.50	19	55	475	0.02	0.07
15 Dec	2033–2147	39	NC	0.94	-7.2	-14.1	0.4	1.8	649	247	0.18	0.48	17	62	450	0.02	0.05
15 Dec	2224–2231	6	NC	0.18	-7.2	-9.1	1.1	1.7	573	227	0.22	0.41	17	33	337	0.01	0.02
19 Dec	1805–1915	25	NC	0.88	-10.0	-13.6	1.1	2.7	219	192	0.23	0.43	18	57	562	0.02	0.09
6 Jan	2111–2355	111	NC	0.01	-3.6	-12.5	0.4	2.2	173	94	0.18	0.49	24	184	387	0.03	0.23
7 Jan	1800–1847	8	C	0.21	-1.5	-4.2	0.3	2.6	520	123	0.08	0.35	24	414	1300	0.01	0.04
7 Jan	2122–2141	12	NC	0.48	-5.5	-6.0	3.6	4.0	477	89	0.32	0.49	24	91	412	0.02	0.06
7 Jan	2153–2208	16	C	0.16	-0.9	-6.9	0.3	3.8	498	34	0.23	0.51	162	379	675	0.12	0.26
8 Jan	1932–2359	91	C	0.10	-0.8	-7.2	0.3	3.6	101	32	0.09	0.25	351	924	1700	0.07	0.24
9 Jan	2019–2021	2	C	0.00	-4.0	-5.7	0.5	1.0	529	297	0.08	0.38	18	23	275	0.03	0.30
9 Jan	2214–2300	39	C	0.12	-1.1	-5.7	0.4	2.1	587	217	0.36	0.78	22	227	1100	0.08	0.30
15 Jan	1829–1958	28	NC	0.53	-2.8	-3.9	0.7	1.7	1125	303	0.24	0.44	18	36	625	0.02	0.06
15 Jan	2039–2050	10	NC	0.99	-8.1	-10.7	2.1	3.2	650	137	0.09	0.30	17	201	375	0.02	0.04
17 Jan	2049–2125	5	NC	0.60	-10.9	-12.0	2.2	2.6	91	60	0.23	0.40	19	25	375	0.00	0.01
22 Jan	2010–2306	56	NC	0.23	-3.6	-10.7	0.6	2.7	1400	290	0.15	0.47	22	135	487	0.01	0.05
23 Jan	1613–1707	8	NC	0.13	-9.7	-14.3	3.5	4.7	64	16	0.08	0.15	26	37	262	0.01	0.02
23 Jan	1817–1939	58	C	0.38	-1.3	-4.0	0.5	2.3	536	61	0.10	0.30	404	908	1700	0.11	0.26
24 Jan	1611–1625	5	NC	0.00	-4.4	-5.2	1.9	2.1	130	138	0.10	0.17	14	24	150	0.00	0.01
24 Jan	1653–1735	14	NC	0.79	-6.1	-10.0	1.1	1.8	779	265	0.15	0.30	16	36	250	0.00	0.01
2 Feb	1940–2040	18	NC	0.94	-8.5	-13.3	1.4	3.1	385	191	0.16	0.45	19	169	475	0.02	0.09
17 Feb	1634–2044	29	NC	0.71	-14.9	-21.6	1.9	6.1	175	15	0.12	0.29	31	116	412	0.01	0.11
18 Feb	1554–1617	6	C	0.00	-0.3	-1.3	0.8	2.0	266	70	0.10	0.23	348	1032	1700	0.03	0.07
18 Feb	2312–0124	50	NC	0.05	-2.2	-4.7	0.7	2.5	315	104	0.25	0.65	24	126	450	0.01	0.05

TABLE 3. Summary of the meteorological conditions associated with each of the 39 SLD environments depicted in Table 2.

Date	Time	Synoptic condition	Notes
CFDE-I cases with SLD			
2 Mar	1741	Warm front	Flight in low stratus below 0°C warm-frontal surface
3 Mar	1917	Warm front precipitation band	Flight in lower cold layer and base of melting layer
6 Mar	2043	Weakening warm front	Flight in melting layer
7 Mar	1656	Warm front	Low stratus behind surface frontal region
9 Mar	1652	Warm front	Cloud was mainly below 0°C surface, -10°C bases
10 Mar	1557	Warm front	Flight in and below melting layer
10 Mar	1900	Low pressure region	Cloud to south of center of low
14 Mar	1625	Warm front freezing rain band	Flight in cloud to northeast of freezing rain band
14 Mar	1803	Warm front	Flight in and below melting layer
14 Mar	1831	Warm front	Flight ahead of surface warm-frontal region
15 Mar	1857	Stationary front	Flight to south of frontal region
17 Mar	1538	Southeast flow	Flow off the sea ice and ocean, adiabatic LWC
18 Mar	1607	Low pressure region	Flight to north of low, in and below melting layer
18 Mar	1842	Low pressure region	Flight to north of low
22 Mar	1450	Warm front	Flight in region of uplifting above front
22 Mar	1706	Warm front	Cloud to north of frontal precipitation region
CFDE-III cases with SLD			
11 Dec	2151	Low region	Long-lived stratus deck to north of low; inversion at top
15 Dec	2033	Warm front	Low stratus cloud ahead of surface front
15 Dec	2224	Warm front	Cloud ahead of surface front; inversion at top
19 Dec	1805	Low pressure region	Midstratus with inversion at top; warm front to north
6 Jan	2111	Warm front, ice storm	Classical profile; cloud top at base of melting layer
7 Jan	1800	Warm front, ice storm	Precipitation band; deep melting layer; cloud above
7 Jan	2122	Warm front, ice storm	Precipitation band; flight in upper cold layer
7 Jan	2153	Warm front, ice storm	Flight at and below base of melting layer
8 Jan	1932	Warm front, ice storm	Melting layer to 9°C; ice nucleation below
9 Jan	2019	Warm front, ice storm	Low stratus had top in melting layer; rain from above
9 Jan	2214	Warm front, ice storm	Precipitation band; ice nucleation below melting layer
15 Jan	1829	Warm front	North of surface front; both formation mechanisms
15 Jan	2039	Warm front	North edge of surface front; above melting layer
17 Jan	2049	Low pressure region	Midstratus deck ahead of system
22 Jan	2010	Low pressure region	Stratus deck ahead of system; lower air very polluted
23 Jan	1613	Low pressure region	Midlevel stratus deck ahead of strong system
23 Jan	1817	Warm front	Freezing rain band; surface temperature of -8°C
24 Jan	1611	Low pressure region	Midlevel stratus deck well behind system
24 Jan	1653	Low pressure region	Stratus deck well behind system
2 Feb	1940	Low pressure region	Stratus well to east of weak low
17 Feb	1634	Low pressure region	High-level stratus deck north of approaching system
18 Feb	1554	Warm front	Below melting layer in back edge of freezing rain band
18 Feb	2312	Warm front	Stratus well behind frontal region

TABLE 4. Statistics for the 39 SLD environments observed during CFDE I and CFDE III. The data are averaged by project and formation mechanism. The averages are based on one value for each SLD environment depicted in Table 2, regardless of the duration. The ± values represent the standard deviations.

Project Formation mechanism	CFDE I C	CFDE I NC	CFDE III C	CFDE III NC
No. of SLD regions	5	11	7	16
Time in SLD conditions (min)	137	379	220	453
Mean duration (min)	27	34	31	28
Mean LWC (g m <sup>-3</sup> )	0.12 ± 0.03	0.14 ± 0.05	0.18 ± 0.10	0.18 ± 0.06
Mean max LWC (g m <sup>-3</sup> )	0.30 ± 0.08	0.31 ± 0.13	0.40 ± 0.18	0.40 ± 0.13
Mean temperature (°C)	0.4 ± 1.4	-2.9 ± 3.1	-1.4 ± 1.1	-6.8 ± 3.3
Mean min temperature (°C)	-2.9 ± 2.3	-5.7 ± 3.4	-5.0 ± 1.9	-10.7 ± 4.3
Mean concentration (cm <sup>-3</sup> )	48 ± 40	48 ± 37	119 ± 94	164 ± 92
Mean mixed-phase conditions (%)	0.12 ± 0.13	0.21 ± 0.32	0.14 ± 0.12	0.49 ± 0.35
Mean MVD (μm)	66 ± 54	33 ± 11	190 ± 162	20 ± 4
Mean max MVD (μm)	720 ± 319	124 ± 96	558 ± 364	87 ± 59
Mean LWC > 50 μm	0.05 ± 0.02	0.03 ± 0.02	0.06 ± 0.04	0.01 ± 0.01
Mean max LWC > 50 μm	0.15 ± 0.04	0.12 ± 0.09	0.17 ± 0.11	0.06 ± 0.05
SLD altitude range (km)	1.5 ± 0.6	1.4 ± 1.1	2.0 ± 1.0	1.4 ± 0.9

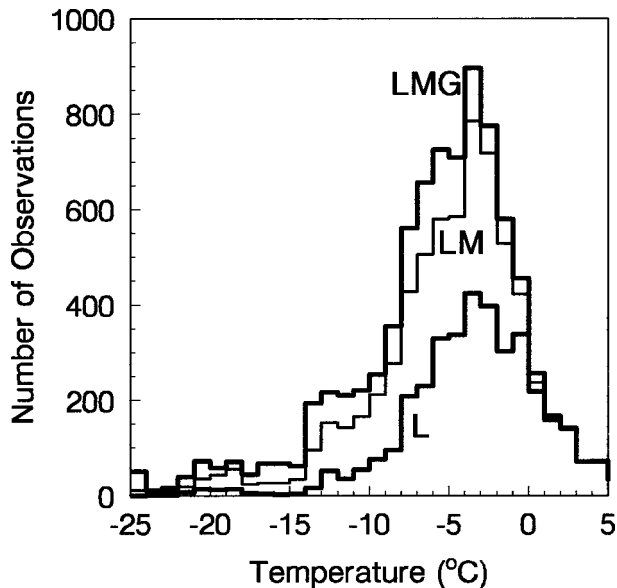


FIG. 1. Histogram of temperature observations between 5° and -25°C collected during CFDE I and III. Each observation represents a 30-s average. The lower curve (L) represents liquid-phase conditions (3618 observations). The middle curve (LM) represents liquid- and mixed-phase conditions (6570 observations), and the upper curve (LMG) represents all in-cloud (i.e., liquid, mixed, and glaciated) conditions (8044 observations).

were insufficient data at temperatures less than -14°C to infer characteristics at these temperatures. The majority of liquid- and mixed-phase measurements with temperatures less than -14°C were made during a single flight on 17 February 1998. The temperature data may represent biases inherent in research flights, in that flights were designed to target regions with aircraft icing and were therefore directed into regions with temperatures between 0° and -15°C. Although the measurements at temperatures greater than 0°C might not be classified as aircraft icing, for classical cases they are probably indicative of an icing environment at a lower altitude. This is because these measurements were primarily made in the melting layer of a warm frontal structure, and it is conceivable that similar conditions existed at subfreezing temperatures in a lower layer. Regardless, the data with temperatures greater than 0°C are not used in the analysis of icing environments. The relative frequencies of observed liquid, mixed, and glaciated cases are discussed in Cober et al. (2001a). The frequency of glaciated cases was a minimum near 0°C and increased steadily with decreasing temperature, whereas the frequency of liquid-phase cases was a maximum near 0°C and decreased with decreasing temperature. The fraction of mixed-phase cases was relatively constant from 0° to -20°C. Overall, approximately 40% of the 30-s observations were assessed as liquid phase, with 40% assessed as mixed phase, and 20% assessed as glaciated phase.

Histograms of droplet concentrations measured in liq-

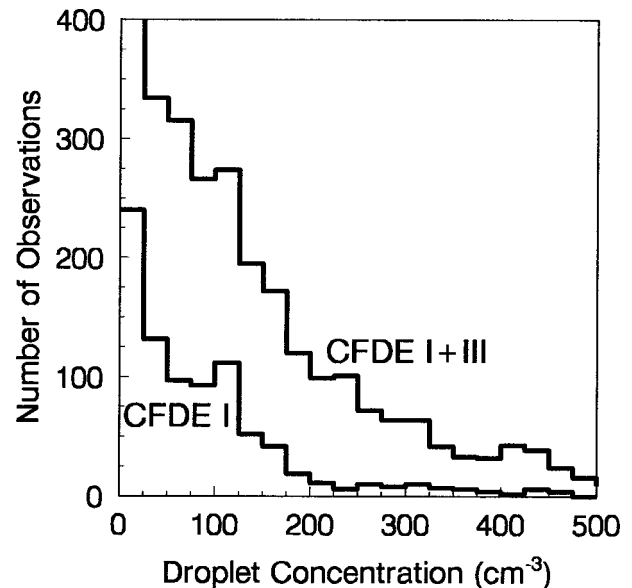


FIG. 2. Histogram of droplet concentration measurements for CFDE-I and -III clouds that were liquid phase with temperatures  $\leq 0^\circ\text{C}$ . The lower curve represents measurements from CFDE I (861 observations); the upper curve represents the collective CFDE-I and -III dataset (2777 observations).

uid-phase clouds for CFDE I and III are shown in Fig. 2. In general, CFDE-I clouds had significantly lower droplet concentrations and interstitial aerosol concentrations (as measured with the PCASP) than CFDE-III clouds. This was consistent with CFDE-I measurements being made in a maritime environment and CFDE-III measurements being made in a continental environment. However, there were several observations of low droplet concentrations during CFDE III, and 5 of the 16 non-classical SLD environments listed for CFDE III in Table 2 had average droplet concentrations of less than 100  $\text{cm}^{-3}$ . Low drop concentrations ( $<100 \text{ cm}^{-3}$ ) account for 39% of the CFDE-III measurements shown in Fig. 2. Politovich (1989), Cober et al. (1996), and Hobbs and Rangno (1996) have discussed the link between clouds with low droplet concentrations and the formation of SLD. Figure 3 shows the concentrations of ice crystals greater than or equal to 125  $\mu\text{m}$  in diameter for mixed and glaciated clouds observed during CFDE I and III. Based on the 30-s in-cloud observations, 94% of the mixed- and glaciated-phase clouds had ice-crystal concentrations of less than 20  $\text{L}^{-1}$ . Ice-crystal concentrations less than 1  $\text{L}^{-1}$  were observed in 48% of the mixed-phase data. These cases generally had an ice water fraction close to 0, with the bulk of the hydrometeor mass incorporated in cloud drops less than 30  $\mu\text{m}$ . In a water-saturated environment, the ice crystals would rapidly grow to sizes greater than 200  $\mu\text{m}$ , and in the absence of an ice multiplication mechanism there would be relatively few smaller ice crystals. This is convenient for measuring the hydrometeor spectra, because a small concentration of large ice crystals combined with rel-

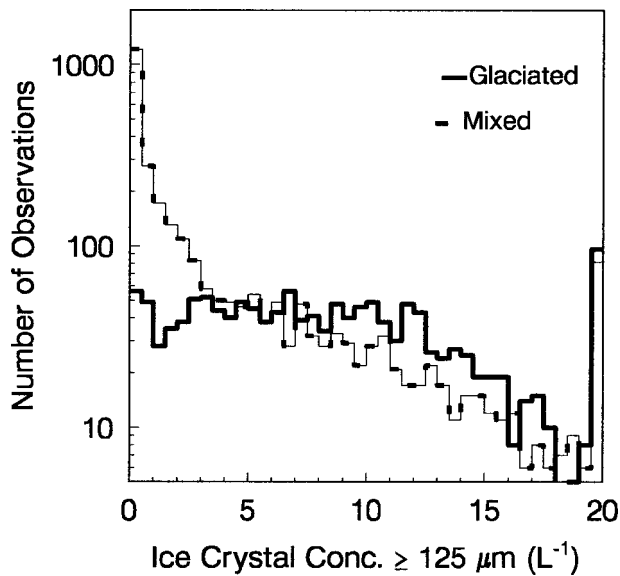


FIG. 3. Histogram of ice-crystal concentrations for CFDE-I and -III clouds with temperatures  $< 0^{\circ}\text{C}$ . The ice crystal concentrations represent 30-s averages of particles  $\geq 125 \mu\text{m}$ . The solid curve represents glaciated-phase cases (1509 observations), and the dashed curve represents mixed-phase cases (2925 observations). All cases with ice-crystal concentrations  $> 20 \text{ L}^{-1}$  are included in the last bin.

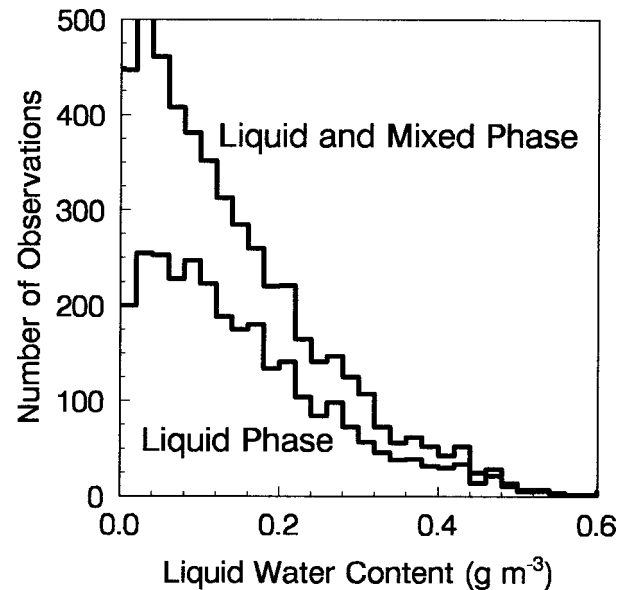


FIG. 4. Histogram of LWC measurements for CFDE-I and -III clouds with temperature  $\leq 0^{\circ}\text{C}$ ,  $\text{LWC} > 0.005 \text{ g m}^{-3}$ , and ice-crystal concentrations  $< 3 \text{ L}^{-1}$ . The LWC values were based on the Nevzorov LWC and TWC measurements averaged over 30 s. The lower curve represents liquid-phase cases (2934 observations); the upper curve represents liquid- and mixed-phase cases (5011 observations).

atively large concentrations of cloud drops would presumably cause minimal contamination of the FSSP measurements and more accurate shape recognition for the 2D images. This may partly explain why there was minimal observed contamination of the FSSP spectra for cloud regions with ice crystal concentrations less than  $1 \text{ L}^{-1}$ .

Figure 4 shows histograms of the LWC measurements for the CFDE-I and -III data. The data represent averages over 30 s for liquid- and mixed-phase conditions, with LWC greater than  $0.005 \text{ g m}^{-3}$ , temperature less than  $0^{\circ}\text{C}$ , and  $C$  less than  $3 \text{ L}^{-1}$ . Only 0.1% of the data had LWC greater than  $0.7 \text{ g m}^{-3}$ , which is similar to the results of Sand et al. (1984). They reported that 0.1% of data collected in winter Great Lakes clouds had LWC greater than  $0.6 \text{ g m}^{-3}$ . The dropoff in frequency with increasing LWC is very similar to the results of Sand et al. (1984) and to those of Cober et al. (1995) for measurements taken during CASP II.

Cober et al. (1995) found that LWC greater than  $0.025 \text{ g m}^{-3}$  at temperatures less than  $0^{\circ}\text{C}$  were observed for only 9% of the in-flight time during 31 CASP-II flights into winter clouds measured off the East Coast in the vicinity of Newfoundland. For the 38 flights in CFDE I and CFDE III, similar conditions were observed during 29% of the in-flight time. Aircraft-icing environments were deliberately targeted on only 14 of the 31 CASP-II flights reported by Cober et al. (1995), versus all 38 of the CFDE flights. CASP-II flights were generally directed into deep synoptic winter storms, whereas CFDE flights were generally directed into stratus clouds

ahead of and behind the frontal precipitation bands of synoptic winter storms. This demonstrates that the relative frequencies of parameters such as LWC can be significantly biased by the research flight methodology.

## 8. Analyses and discussion

### a. Assessing the LWC of the drop spectra

The cloud drop spectra, based on combining measurements from the two FSSPs, 2D-C, and 2D-P probes, were determined for each 30-, 60-, 120-, and 300-s average. Parameters such as LWC, MVD, and 80VD could then be determined for each integrated spectrum. To assess the quality of the data, the LWC determined from each drop spectrum was compared with the measured LWC. Because the King and Nevzorov LWC instruments have a significant falloff in response for drops greater than  $100 \mu\text{m}$  (Biter et al. 1987; Strapp et al. 2000), they were not used in the comparison. However, the Nevzorov TWC instrument is not believed to suffer this limitation (Strapp et al. 2000) and therefore was used for the comparison. A comparison between the measured LWC and integrated LWC is shown in Fig. 5 for liquid- and mixed-phase cases with  $C$  less than  $1 \text{ L}^{-1}$ . The best fit (not shown) has a slope of 1.06, which demonstrates a good agreement between the measurements. The integrated LWC has an estimated error of approximately 40% (Cober et al. 2001a; Baumgardner 1983), and the Nevzorov TWC has an error of  $\pm 15\%$ , for a combined error of 43% (Baumgardner 1983). The

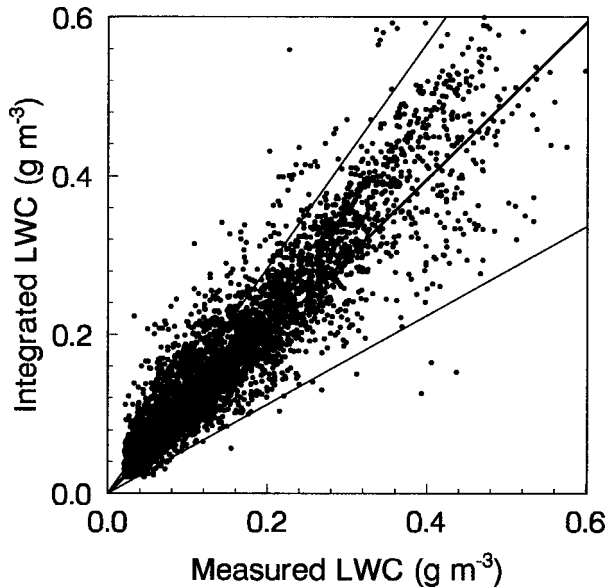


FIG. 5. Scatterplot of measured LWC vs the integrated-spectrum LWC for each 30-s measurement. The data represent 4840 liquid- and mixed-phase observations with  $LWC > 0.01 \text{ g m}^{-3}$  and  $C < 1 \text{ L}^{-1}$ . The solid curves represent a 1:1 correlation and  $\pm 43\%$  to the 1:1 correlation. The measured LWC was based on the Nevzorov LWC and TWC measurements.

1:1 correlation and  $\pm 43\%$  curves are shown in Fig. 5 and contain 90% of the data with LWC greater than  $0.1 \text{ g m}^{-3}$ . Another comparison can be made with the RID LWC. Cober et al. (2001b) showed that the RID was capable of estimating LWC to within  $\pm 50\%$  for  $T_a$  less

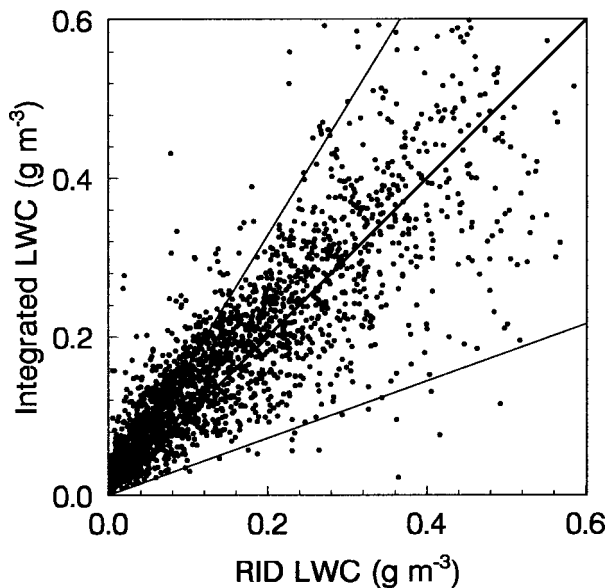


FIG. 6. Scatterplot of LWC inferred from the RID vs the integrated-spectrum LWC for each 30-s measurement. The data represent 2250 liquid- and mixed-phase cases with  $T_a < -4^\circ\text{C}$  and  $C < 1 \text{ L}^{-1}$ . The solid curves represent a 1:1 correlation and  $\pm 64\%$  to the 1:1 correlation.

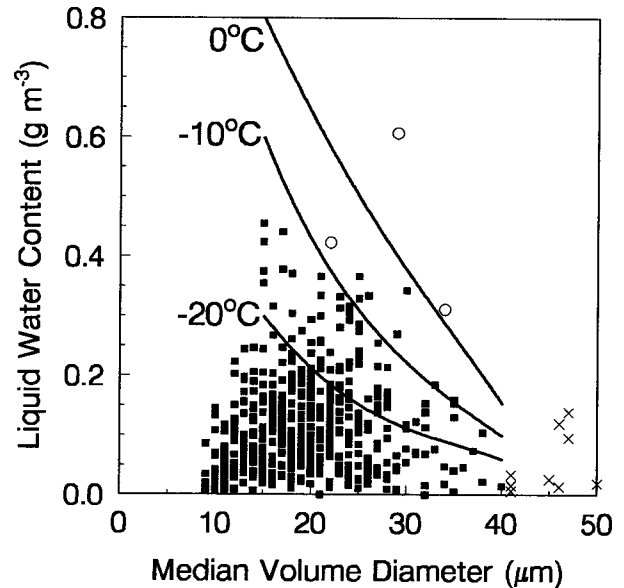


FIG. 7. Plot of MVD vs LWC for 300-s averaged data. MVD is determined from the integrated drop spectrum; LWC is determined from the Nevzorov TWC and LWC measurements. The data represent liquid- and mixed-phase cases with  $T_a \leq 0^\circ\text{C}$ ,  $C < 1 \text{ L}^{-1}$ , and  $MVD < 40 \mu\text{m}$  (527 cases). The solid curves represent the FAR 25-C curves for  $0^\circ$ ,  $-10^\circ$ , and  $-20^\circ\text{C}$ . Open circles represent the three cases in which the MVD-LWC values exceeded the FAR 25-C curves that corresponded to the measurement temperature. The  $\times$  symbols represent some of the 47 cases that had  $MVD > 40 \mu\text{m}$ .

than  $-4^\circ\text{C}$  and LWC values below the Ludlam limit. They also showed that the RID was capable of measuring LWC within  $\pm 50\%$  for cases with high MVD. With an integrated LWC error of  $\pm 40\%$  and an RID LWC error of  $\pm 50\%$ , a comparison should show agreement within  $\pm 64\%$ . Figure 6 shows a comparison between the RID and integrated-spectra LWC. The data are scattered along the 1:1 curve, and 90% of the data fall within the  $\pm 64\%$  curves. The good agreement between the Nevzorov TWC, RID LWC, and integrated-spectra LWC within the errors expected for such comparisons provides confidence in the measurements and is indicative that the spectra contain reasonable values.

#### b. Comparison with the FAR 25-C icing envelopes

The 300-s averages were determined in order to compare the data with the FAR 25-C curves for maximum continuous icing. The FAR 25-C curves represented extreme or worst-case environments for horizontal lengths of approximately 33 km, which is close to the 30-km average length scale for the 300-s averaged data. At 300-s resolution, the CFDE dataset contained 1848 in-flight data points, of which 993 were assessed as being in cloud. The 300-s data for liquid- and mixed-phase cases with MVD less than  $40 \mu\text{m}$ ,  $C$  less than  $1 \text{ L}^{-1}$ , and  $T_a$  less than or equal to  $0^\circ\text{C}$  are shown in Fig. 7 (527 cases), along with the FAR 25-C curves for  $0^\circ$ ,

$-10^{\circ}$ , and  $-20^{\circ}\text{C}$ . The data with MVD less than  $40\ \mu\text{m}$  were segregated because the FAR 25-C curves are only defined to  $40\ \mu\text{m}$ . There were three data points that had LWC–MVD–temperature values that exceeded the FAR 25-C curves (shown as open circles in Fig. 7) and an additional 47 data points with MVD greater than  $40\ \mu\text{m}$  (shown as  $\times$  symbols). These represent 0.5% and 8%, respectively, of the cases shown in Fig 7; 0.3% and 4.7%, respectively, of the in-cloud observations; and 0.2% and 2.5%, respectively, of the in-flight observations made during CFDE flights. Assuming that the frequency of exceedence for the CFDE dataset should be significantly higher than that expected for randomly collected data, it can be concluded that the FAR 25-C curves are consistent with 0.1% exceedence probabilities for MVD less than  $40\ \mu\text{m}$ . However, it can also be concluded that because 2.5% of the in-flight CFDE 300-s measurements have MVD greater than  $40\ \mu\text{m}$ , the FAR 25-C curves do not adequately represent the full icing environments observed in nature.

### c. Comparison with the Politovich hazardous icing conditions

The LWC and MVD were determined for each 30-s data point. There were 18 480 in-flight observations, of which 8132 were determined to be in cloud. Of these, there were 2793 liquid- and mixed-phase observations with  $T_a$  less than or equal to  $0^{\circ}\text{C}$ ,  $D_{\text{max}}$  greater than or equal to  $50\ \mu\text{m}$ , and  $C$  less than  $1\ \text{L}^{-1}$ . These were considered to represent SLD conditions for which the drop spectra measurements were not significantly biased by ice-crystal contamination.

There were 87 observations with MVD greater than  $30\ \mu\text{m}$  and LWC greater than  $0.2\ \text{g m}^{-3}$ , which correspond to conditions that Politovich (1996) described as having the greatest detrimental effects on aircraft performance. This set represents 3.1% of the observed SLD conditions, 1.1% of the observed in-cloud conditions, or 0.5% of the in-flight observations. Each 30-s SLD observation was associated with either a classical or nonclassical formation mechanism. The relative percentages of classical and nonclassical SLD observations that met the Politovich hazardous conditions criteria were 4.8% and 2.5%, respectively. This result suggests that there were no significant differences between the formation mechanisms with respect to the probability of developing hazardous icing conditions as described by Politovich (1996).

### d. Comparison with the Newton icing envelopes

The 30-s LWC and MVD pairs for 2765 SLD observations are plotted in Fig. 8 and are compared with the potential accumulation curves given by Newton (1978). The data are segregated by formation mechanism. MVD values to  $1000\ \mu\text{m}$  were observed in classical formation conditions and represent measurements

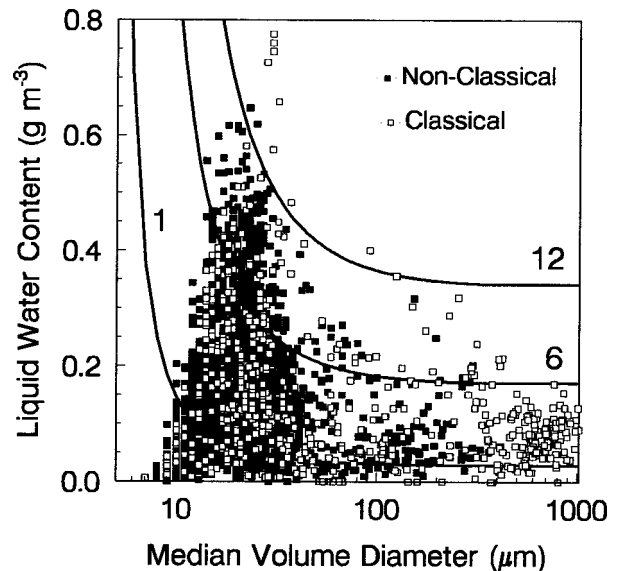


FIG. 8. Plot of MVD vs LWC for each 30-s observation that included SLD. The data are segregated by formation mechanism and represent classical (569 points) and nonclassical (2196 points) cases with  $T_a \leq 0^{\circ}\text{C}$ ,  $D_{\text{max}} \geq 50\ \mu\text{m}$ , and  $C < 1\ \text{L}^{-1}$ . The solid curves represent potential accumulation curves for 1, 6, and  $12\ \text{g cm}^{-2}\ \text{h}^{-1}$ , as defined by Newton (1978).

made below cloud base in freezing rain. There were no nonclassical cases with MVD greater than  $400\ \mu\text{m}$ . The cases with MVD greater than  $400\ \mu\text{m}$  were primarily obtained when the aircraft was flying below cloud base and below a melting layer. For the cases with MVD less than  $400\ \mu\text{m}$ , there is little difference between the classical and nonclassical cases. For classical cases with MVD less than  $400\ \mu\text{m}$ , the measurements were often made in stratiform clouds within the lower cold layer. The combination of SLD from the melting layer and cloud drops from the lower stratiform cloud could blur any distinctive characteristics between classical and nonclassical cases. Newton classified potential accumulations of 6 and  $12\ \text{g cm}^{-2}\ \text{h}^{-1}$  as representative of moderate and severe icing conditions, respectively. For the SLD observations formed through classical and nonclassical mechanisms, 13% and 16%, respectively, had potential accumulations of greater than  $6\ \text{g cm}^{-2}\ \text{h}^{-1}$ . This result demonstrates no significant differences between formation mechanisms with respect to the probability of developing moderate or severe icing conditions as described by Newton (1978).

Figure 9 shows the same data as Fig. 8, with the data segregated by cloud phase. There are no significant differences in the data for the liquid- and mixed-phase cases for MVD less than  $50\ \mu\text{m}$ . However, for MVD greater than  $50\ \mu\text{m}$ , virtually every case with a potential accumulation of greater than  $6\ \text{g cm}^{-2}\ \text{h}^{-1}$  was liquid phase. One possible explanation is that the presence of ice crystals will result in the freezing of drizzle-sized drops, which will lower the LWC and MVD. Increased collision efficiency of large drops with ice crystals and

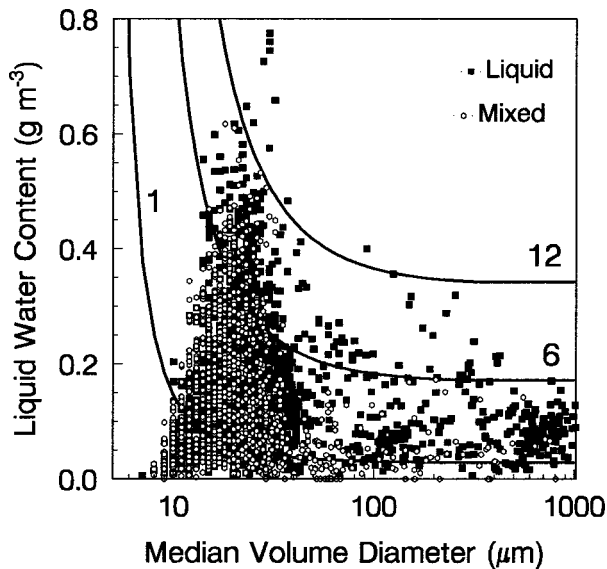


FIG. 9. Plot of MVD vs LWC for the same conditions as in Fig. 8, except that the data are segregated by cloud phase. There are 1623 and 1142 liquid- and mixed-phase cases, respectively.

the relationship between large drops and ice multiplication (Hallett and Mossop 1974) are consistent with this hypothesis. The cases with MVD of greater than  $400 \mu\text{m}$  tended to be primarily liquid phase, which is consistent with being measured below a melting layer at temperatures greater than  $-5^\circ\text{C}$ . There were an additional 1845 liquid- and mixed-phase data points that had  $D_{\text{max}}$  less than  $50 \mu\text{m}$  (i.e., non-SLD cases). These cases were not shown in Fig. 9; however, the data are very similar to the cases in Fig. 9 with MVD less than  $40 \mu\text{m}$ . Of the 4610 SLD and non-SLD icing cases with  $T_a$  less than or equal to  $0^\circ\text{C}$ , there were 463 (10%) with MVD greater than  $40 \mu\text{m}$ , which were therefore outside of the FAR 25-C envelopes.

Figure 10 shows the same data segregated by temperature. The extreme MVD and LWC values all have  $T_a$  greater than  $-7^\circ\text{C}$ , although there are insufficient data points at extreme values to conclude that these situations do not occur at temperatures colder than  $-7^\circ\text{C}$ . Cases with temperatures in the lower cold layer as cold as  $-10^\circ\text{C}$  have been observed (Zerr 1997) in classical formation environments. There is an expectation that the average and extreme LWC values will decrease with decreasing temperature, as is demonstrated by the FAR 25-C curves. However, there are insufficient data in the CFDE dataset to assess this expectation accurately. On 17 February 1998, a case with MVD of  $31 \mu\text{m}$ , LWC of  $0.22 \text{ g m}^{-3}$ , and drops to  $400 \mu\text{m}$  was observed at  $-20.8^\circ\text{C}$  at an altitude of 6 km. The cloud was a widespread stratus deck, which lasted several hours (as observed by satellite) and had no overlying cloud. The associated icing caused a tail buffet on the aircraft, and ice was observed to completely bridge over the heated portion of the tail. Surface measure-

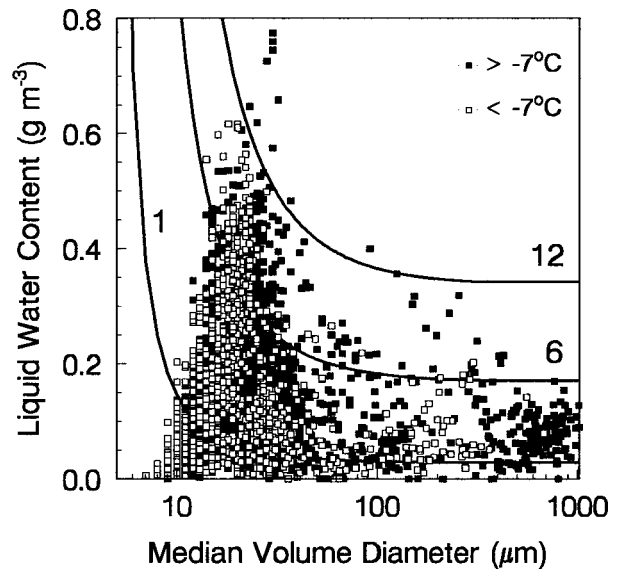


FIG. 10. Plot of MVD vs LWC for the same conditions as in Fig. 8, except that the data are segregated by temperature. There are 1955 points with  $0 \geq T_m -7^\circ\text{C}$  and 892 points with  $T_m \leq -7^\circ\text{C}$ , where  $T_m$  represents the minimum temperature observed in each 30-s interval.

ments of SLD at temperatures of  $-20^\circ\text{C}$  have been observed by Kajikawa et al. (2000), who inferred that the source regions for the SLD could have been as warm as  $-7^\circ$  to  $-10^\circ\text{C}$ . The source regions on 17 February 1998 were at approximately  $-21^\circ\text{C}$ .

The data shown in Figs. 8 to 10 can be segregated by MVD for discussion. For cases with MVD less than  $50 \mu\text{m}$ , the potential accumulation curves change rapidly because of the large change in collision efficiency with diameter for diameters less than  $40 \mu\text{m}$ . A potential accumulation of  $12 \text{ g cm}^{-2} \text{ h}^{-1}$  bounds 99.5% of the SLD data in this range. The LWC for these cases is primarily incorporated into small cloud drops, although substantial LWC may still exist in larger drops. This is one of the disadvantages of representing the data by only LWC and MVD. For droplets greater than  $50 \mu\text{m}$ , the collision efficiency approaches 1, so that the potential accumulation curves level off. For CFDE cases with  $50 < \text{MVD} < 400 \mu\text{m}$ , the drop spectrum mass was normally observed to be incorporated into two modes, including a droplet mode between 10 and  $30 \mu\text{m}$  and a drizzle mode between 100 and  $400 \mu\text{m}$ . The MVD may be variable in these cases, although this is of little concern when the data are plotted against a potential accumulation curve, because the curves are essentially flat. For the data with MVD greater than  $50 \mu\text{m}$ , the potential accumulation curve of  $12 \text{ g cm}^{-2} \text{ h}^{-1}$  bounds 99.8% of all the 30-s averages. When the MVD is greater than  $400 \mu\text{m}$ , the majority of the droplet mass is incorporated into rain- and drizzle-sized drops. A potential accumulation of  $6 \text{ g cm}^{-2} \text{ h}^{-1}$  bounds all the data points observed with MVD greater than  $400 \mu\text{m}$ . There

is some indication in the data that the maximum LWC values decrease with increasing MVD; however, considerable additional data will need to be collected before this can be fully substantiated. Overall, 84% of the 30-s SLD observations are bounded by the  $6 \text{ g cm}^{-2} \text{ h}^{-1}$  potential accumulation curve, whereas the extreme values are close to the  $12 \text{ g cm}^{-2} \text{ h}^{-1}$  curve. When the data are presented in a format similar to that shown in Fig. 8 except using diameter measurements such as 80VD, there are no differences in the interpretation. This occurs because for MVD less than  $50 \mu\text{m}$  the MVD and 80VD are usually very close, whereas for MVD greater than  $50 \mu\text{m}$  the potential accumulation curves are flat and are independent of diameter. Hence 80VD or other diameter-related parameters provide no better description than MVD in this kind of analysis.

*e. Comparison with the Ashenden and Marwitz envelopes*

Ashenden and Marwitz (1998) assessed the number of encounters per hour for which the LWC incorporated in drizzle-sized drops ( $44\text{--}194 \mu\text{m}$  in diameter) exceeded thresholds of  $0.05$ ,  $0.10$ , and  $0.30 \text{ g m}^{-3}$ . They determined the drizzle water content using a 1D probe in conditions for which minimal ice-crystal contamination was assessed. They further screened data with temperatures greater than  $-1^\circ\text{C}$  and with significant mass in precipitation-sized drops (i.e., freezing-rain conditions). The CFDE data are compared with the envelopes derived by Ashenden and Marwitz (1998) and are shown in Fig. 11. For the CFDE measurements, the LWC incorporated in drops greater than  $50 \mu\text{m}$  was used to represent the drizzle water content and data with temperatures greater than  $-1^\circ\text{C}$  were screened out. No attempts were made to exclude freezing-rain conditions. Encounters per flight-hour were determined by using the number of 30-, 60-, 120-, and 300-s observations that exceeded the drizzle LWC thresholds and the fact that there were 154 in-flight hours during CFDE I and CFDE III. The CFDE data for drizzle LWC thresholds of  $0.05$  and  $0.10 \text{ g m}^{-3}$  are similar to those of Ashenden and Marwitz (1998), although the CFDE data appear to drop off faster for longer length scales. This is likely related to differences in how the data are averaged. There were no observations during CFDE, on any length scale, for which the drizzle LWC was greater than  $0.3 \text{ g m}^{-3}$ . Ashenden and Marwitz (1998) observed drizzle LWC greater than  $0.3 \text{ g m}^{-3}$  over a 3-km scale at a frequency of 0.6 observations per flight-hour. At this frequency, there would have been 92 such observations during CFDE. There is no clear explanation for the differences between the two field projects. Assuming no systematic differences in the analysis techniques, these observations would imply that the Sierra Nevada and Front Range Rockies clouds observed by Ashenden and Marwitz (1998) have a significantly higher potential for producing extreme icing

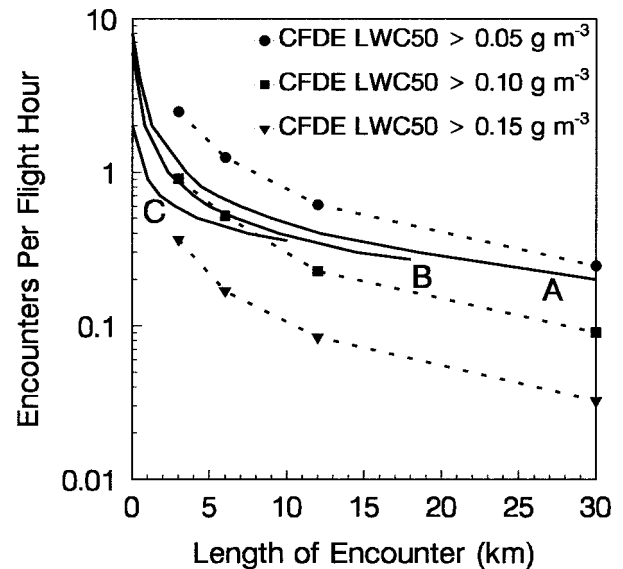


FIG. 11. Plot of encounter length vs encounters per flight hour for SLD conditions. The solid curves A, B, and C represent the results of Ashenden and Marwitz (1998) for drizzle LWC thresholds of  $0.05$ ,  $0.10$ , and  $0.30 \text{ g m}^{-3}$ , respectively. The dashed curves represent analysis of the CFDE observations for SLD thresholds of  $0.05$ ,  $0.10$ , and  $0.15 \text{ g m}^{-3}$ . LWC50 represents the LWC incorporated in drops  $> 50 \mu\text{m}$  in diameter.

conditions than the Great Lakes and North Atlantic clouds observed during CFDE. Ashenden and Marwitz (1998) computed the  $80\text{VD} \times \text{LWC}$  values ( $\mu\text{m g m}^{-3}$ ) for each icing region and assessed values between 10 and 100 as having the largest performance degradation on their Super King-Air aircraft. For the 2793 30-s SLD cases observed during CFDE, 29% had  $80\text{VD} \times \text{LWC}$  between 10 and  $100 \mu\text{m g m}^{-3}$ , which represents 4.3% of the in-flight observations.

*f. Comparison with the Jeck envelopes*

The 30-s data with  $T_a$  less than or equal to  $0^\circ\text{C}$ ,  $D_{\text{max}}$  greater than or equal to  $50 \mu\text{m}$ , and  $C$  less than  $1 \text{ L}^{-1}$  were used to determine the LWC and droplet concentration percentiles for the diameter bins proposed by Jeck (1996), and the results are presented in Table 5. These percentiles are with respect to flight in SLD conditions. To convert to in-cloud or in-flight percentiles, the values need to be multiplied by 0.34 or 0.15, respectively. The maximum values observed are not shown because of the increased potential for error with single extreme cases. The Nevzorov TWC and integrated LWC for drops greater than  $1 \mu\text{m}$  agree within 16% for all percentile values. The average LWC incorporated in drops greater than  $50 \mu\text{m}$  was  $0.027 \text{ g m}^{-3}$ , with a 99th-percentile value of  $0.2 \text{ g m}^{-3}$ . This is lower than the  $0.3 \text{ g m}^{-3}$  value given by Jeck (1996), who summarized similar measurements reported in the literature. Jones and Lewis (1949) suggested that  $0.15 \text{ g m}^{-3}$  would represent an extreme LWC for freezing pre-

TABLE 5. Percentiles of LWC ( $\text{g m}^{-3}$ ) and droplet number concentration ( $\text{cm}^{-3}$ ) segregated into the diameter intervals proposed by Jeck (1996). The statistics were determined from 2793 30-s averages. Only liquid- and mixed-phase cases for which  $T_a \leq 0^\circ\text{C}$ ,  $D_{\text{max}} \geq 50 \mu\text{m}$ , and  $C < 1 \text{ L}^{-1}$  were used for this analysis.

Range ( $\mu\text{m}$ )	Mean	25%	50%	75%	95%	99%
LWC percentiles						
Nevzorov	0.17	0.079	0.15	0.25	0.42	0.51
>1	0.20	0.094	0.17	0.27	0.46	0.61
>50	0.027	0.0020	0.0084	0.033	0.12	0.20
>100	0.019	0.0	0.0026	0.017	0.11	0.19
>500	0.0061	0.0	0.0	0.0	0.055	0.13
1–50	0.17	0.062	0.13	0.24	0.44	0.58
50–100	0.0079	0.0011	0.0035	0.0097	0.029	0.073
100–200	0.0058	0.0	0.0014	0.0062	0.029	0.047
200–300	0.0036	0.0	0.0002	0.0023	0.018	0.053
300–400	0.0023	0.0	0.0	0.0001	0.013	0.048
400–500	0.0014	0.0	0.0	0.0	0.0095	0.023
500–1000	0.0041	0.0	0.0	0.0	0.036	0.087
1000–1500	0.0018	0.0	0.0	0.0	0.011	0.046
1500–3000	0.0002	0.0	0.0	0.0	0.0	0.010
Droplet concentration percentiles						
>1	140	35	97	201	443	624
>50	0.061	0.0098	0.029	0.073	0.22	0.51
>100	0.0053	0.0	0.0015	0.0062	0.026	0.040
>500	0.0	0.0	0.0	0.0	0.0003	0.0006

precipitation conditions with MVD of  $1000 \mu\text{m}$  and horizontal extent greater than  $100 \text{ km}$ . The CFDE 300-s 99th-percentile value for LWC in drops greater than  $50 \mu\text{m}$  was approximately  $0.16 \text{ g m}^{-3}$ , which is consistent with Jones and Lewis (1949), albeit at a smaller horizontal scale. Pruppacher and Klett (1978) stated that concentrations of drops greater than  $40 \mu\text{m}$  need to exceed a few per liter for a collision-coalescence mechanism to be initiated. For the CFDE data, the average concentration of drops greater than  $50 \mu\text{m}$  was  $61 \text{ L}^{-1}$  and the 95th-percentile value was greater than  $200 \text{ L}^{-1}$ . This result is consistent with the high frequency of SLD cases during CFDE that were inferred to have formed through a nonclassical process.

The length scale over which the data are averaged will influence the values of the percentiles given in Table 5, particularly if the averaging scale is larger than the cloud extent. Figure 12 shows how the percentile values for LWC and concentration change with averaging intervals between 30 and 300 s. The LWC curves are relatively flat, with an approximately 25% difference between the 30- and 300-s averages. This result is not surprising because of the widespread and stratiform nature of many of the clouds that were observed. These results are different than the curves given in FAR 25-C, which attempt to relate the maximum LWC values at different length scales. Based on the FAR 25-C data, an increase in length scale by a factor of 10 reduces the 99th-percentile LWC by approximately 50%, versus a 25% reduction for the results shown in Fig. 12a. Sand et al. (1984) similarly found that an increase in the averaging scale by a factor of 10 reduced their 99th-percentile LWC values by approximately 38%. The dif-

ferences might be related to how clear-air regions are incorporated into the average values. For the CFDE data, the majority (>75%) of data points for all averaging intervals were assessed as being entirely in cloud, which illustrates that the clouds were stratiform with large horizontal extent.

There is a substantial difference between the 90%, 95%, and 99% curves for all parameters shown in Fig. 12. As a consequence, the 99.5% values are also plotted in Fig. 12. The data in Fig. 12 were based on 2742, 1710, 1012, and 509 data points for the 30-, 60-, 120-, and 300-s averages, respectively. To have some confidence in the high-percentile statistics and to avoid errors inherent with interpreting maximum values, it was desired to have in excess of five data points with higher values before quoting a value corresponding to an extreme percentile such as 99.9%. A 99.5% value implied between 14 and 5 data points of higher values, for the 30-, 60-, and 120-s averaging intervals. The 99.5% curves can be taken to represent the extreme values observed in the CFDE dataset. Considerable additional data will be required before the 99.9th-percentile curves can be drawn with confidence.

When the Jeck bins are computed for the 30-s data with  $1 \leq C < 5 \text{ L}^{-1}$ , the mean LWC values for 1–50, 50–100, 100–200, and 500–1000  $\mu\text{m}$  are 0.11, 0.018, 0.0087, and  $0.0007 \text{ g m}^{-3}$ , respectively. These show substantially less mass in the 1–50- and 500–1000- $\mu\text{m}$  ranges and more mass in the 50–100- and 100–200- $\mu\text{m}$  ranges in comparison with the data in Table 5. For the 50–100- and 100–200- $\mu\text{m}$  bins, the increased mass is caused by the FSSP response in channels greater than  $35 \mu\text{m}$ , when ice crystals are present in concentrations

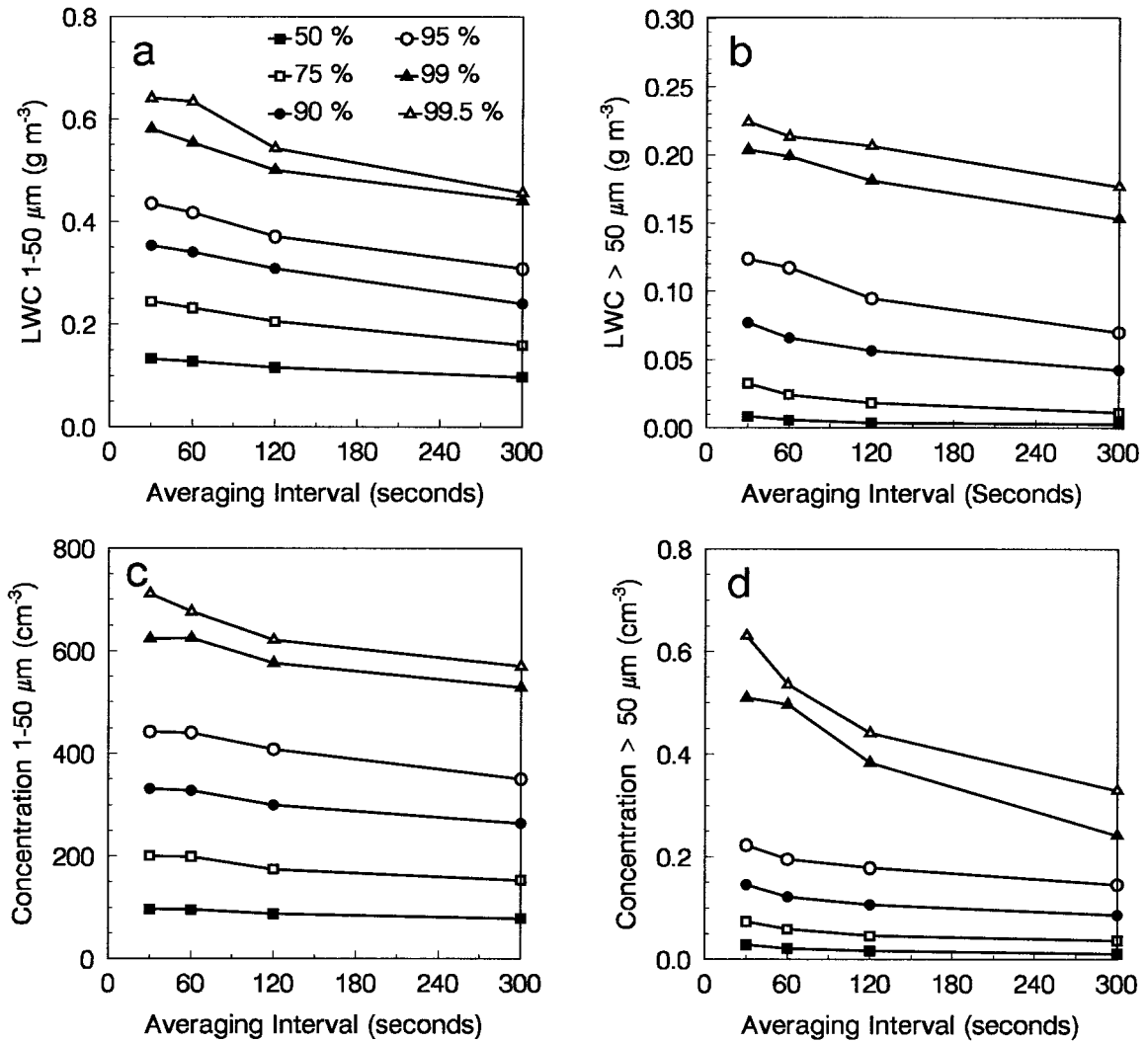


FIG. 12. Change in percentile values with averaging interval for (a) LWC < 50  $\mu\text{m}$ , (b) LWC > 50  $\mu\text{m}$ , (c) droplet concentration < 50  $\mu\text{m}$ , and (d) droplet concentration > 50  $\mu\text{m}$ . The data were calculated using the same criteria used in Table 5. The curves represent the 50th, 75th, 90th, 95th, 99th, and 99.5th percentiles.

greater than  $1 \text{ L}^{-1}$ . There were 723 mixed-phase cases with  $1 \leq C < 5 \text{ L}^{-1}$ , and the MVD–LWC pairs for each case are shown in Fig. 13. The average LWC for the data in Fig. 13 is 37% lower than for the data in Fig. 8. There is a higher percentage of data with MVD between 50 and 100  $\mu\text{m}$  in the mixed-phase cases, which is associated with the FSSP response to ice crystals. The maximum LWC values were lower than in the liquid-phase cases, especially for cases with MVD greater than 50  $\mu\text{m}$ , presumably because the ice crystals were removing liquid water from the clouds. The data in Fig. 13 demonstrate that the errors associated with interpreting FSSP and 2D-C measurements in mixed-phase clouds can be subtle, especially when the data are presented in a bulk LWC and MVD format.

*g. Comparison with formation mechanism theories*

To gain some insight into the nonclassical formation mechanisms for SLD-sized drops, the bulk Richardson number  $Ri$  and shear were computed following Pobanz et al. (1994). Table 2 lists 39 nonclassical environments for which SLD was observed, of which 27 had sufficient vertical profiles of temperature, pressure, and wind vectors to assess  $Ri$  and shear in regions in which SLD was estimated to originate. Pobanz et al. (1994) suggested that  $Ri$  of less than 1 and shear of greater than  $0.02 \text{ s}^{-1}$  were indicative of a dynamically unstable shear layer, which had the potential for maintaining turbulence and mixing and hence the potential for formation of SLD. They showed a statistically significant correlation between shear layers and the formation of large drops. Of

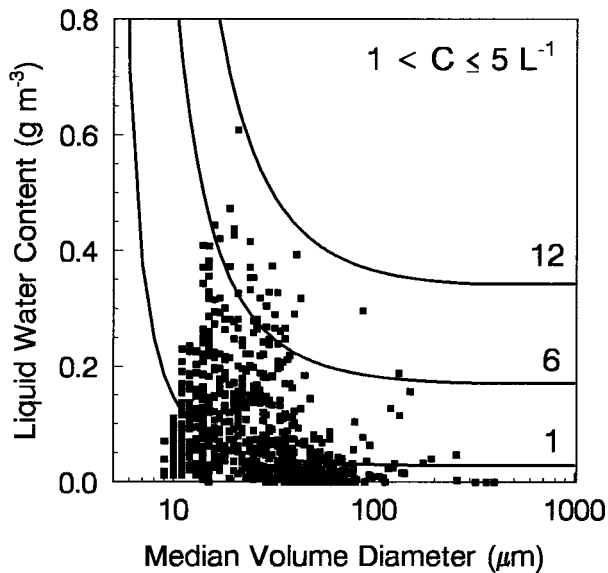


FIG. 13. Plot of MVD vs LWC for each 30-s average with  $T_a \leq 0^\circ\text{C}$ ,  $D_{\text{max}} \geq 50 \mu\text{m}$ , and  $1 \leq C < 5 \text{ L}^{-1}$  (723 data points). The solid curves represent the Newton potential accumulation curves for 1, 6, and  $12 \text{ g cm}^{-2} \text{ h}^{-1}$ .

the 27 CFDE environments with SLD that were examined, 22 had  $R_i$  less than 1 and shear greater than  $0.02 \text{ s}^{-1}$ , which is consistent with the results presented by Pobanz et al. (1994). The remaining five cases all had  $R_i$  greater than 1 and low values of shear; however, in each of these cases a substantial inversion existed at cloud top. An in-cloud or cloud-top inversion was correlated with the SLD formation region in 15 of the 27 cases, with an additional six cases having a weak inversion. Korolev and Isaac (2000) showed how isobaric mixing across a substantial temperature inversion can lead to the growth of large drops through changes in supersaturation. The CFDE results are qualitatively consistent with the Pobanz et al. (1994) and Korolev and Isaac (2000) discussions of formation mechanisms.

## 9. Conclusions

Measurements of icing environments were made during 38 research flights conducted during the First and Third Canadian Freezing Drizzle Experiments. In total, there were 2793 30-s averages obtained in liquid- and mixed-phase clouds with temperatures less than or equal to  $0^\circ\text{C}$ , maximum droplet diameters greater than or equal to  $50 \mu\text{m}$ , and ice-crystal concentrations less than  $1 \text{ L}^{-1}$ . The data also include 39 distinct environments in which supercooled drops of greater than  $50 \mu\text{m}$  were formed either through the classical melting and resupercooling mechanism or through the nonclassical condensation–collision–coalescence mechanism. The majority of data were collected in stratiform winter clouds associated with warm-frontal or low pressure regions. Although analysis of the formation mechanisms is beyond the

scope of this work, the observations are qualitatively consistent with Pobanz et al. (1994) and Korolev and Isaac (2000). It can be argued that the data will include several biases such as temperatures primarily greater than  $-15^\circ\text{C}$ , clouds mainly associated with warm-frontal regions, no flight data in regions of significant convection, icing associated with more extreme meteorological conditions, and a higher frequency of icing detection than for random flights. Regardless, most of the data were obtained in regions with regular air traffic, and the data are directly applicable to icing-related questions currently being considered by several regulatory authorities such as the FAA. The analysis has been presented in a format that is suitable for the aviation community and has led to the following conclusions:

- 1) Integrated drop spectra were determined from four instruments, including FSSP 3–45- $\mu\text{m}$ , FSSP 5–95- $\mu\text{m}$ , 2D-C, and 2D-P probes. The derived LWCs agreed with the measured LWCs from both a Nevzorov LWC–TWC probe and a Rosemount icing detector, within the errors expected from such comparisons. This result provides confidence in the data analysis techniques for determining the integrated spectra. Because each measuring device can have significant error, both in the measurements (i.e., depth-of-field accuracy, fogging, calibrations, icing up, etc.) and in the interpretation of the measurements (i.e., segregating ice and water particles, ice-crystal contamination, etc.), such a comparison is important, especially when extreme values are used for deriving parameters such as exceedance probabilities.
- 2) Based on the 300-s averages, which had comparable length scales to the FAR 25-C curves for continuous maximum icing, the LWC and MVD data for icing conditions with MVD less than  $40 \mu\text{m}$  are consistent with the 99.9th-percentile FAR 25-C exceedance curves. However, the FAR 25-C curves do not exceed  $40 \mu\text{m}$ . Because 8% of the CFDE measurements for which SLD was observed (or 2.5% of all in-flight data) had MVD greater than  $40 \mu\text{m}$ , it is clear that the FAR 25-C curves do not adequately represent all the icing environments found in nature.
- 3) When the data were averaged at 30-s resolution, 99.5% of the data that contained SLD were bounded by the Newton (1978) potential accumulation curve of  $12 \text{ g cm}^{-2} \text{ h}^{-1}$ , independent of the MVD. Eighty-four percent of the data were similarly bounded by a potential accumulation of  $6 \text{ g cm}^{-2} \text{ h}^{-1}$ . The data appear to follow the potential accumulation curves, which is reasonable given that they are more physically based than the other icing envelopes. An LWC of greater than  $0.025 \text{ g m}^{-3}$  was observed during 29% of all in-flight time during the CFDE flights, and LWC greater than  $0.7 \text{ g m}^{-3}$  represented the 99.9th-percentile value. For cases in which drops greater than  $50 \mu\text{m}$  in diameter were observed, the

99th-percentile LWC for SLD sizes was  $0.2 \text{ g m}^{-3}$ . These observations are consistent with other reports of LWC in winter storms (Jones and Lewis 1949; Sand et al. 1984; Cober et al. 1995; Jeck 1996). The maximum MVD values observed were approximately  $1000 \mu\text{m}$  and represented cases in which the aircraft was flown in freezing-rain conditions below cloud base. In one case, SLD were observed to form in a high-altitude stratus cloud at a temperature of  $-21^\circ\text{C}$ .

- 4) The frequency of observed hazardous icing conditions was assessed using several techniques. Icing conditions with MVD greater than  $30 \mu\text{m}$  and LWC greater than  $0.2 \text{ g m}^{-3}$  were assessed in 0.5% of the 30-s in-flight observations. These correspond to conditions that Politovich (1996) described as hazardous. Ashenden and Marwitz (1998) showed that  $\text{MVD} \times \text{LWC}$  values between 10 and  $100 \mu\text{m g m}^{-3}$  were associated with the largest performance degradations for their aircraft. For the CFDE 30-s data, 4.3% of the in-flight measurements met these criteria. Last, 2.5% of the in-flight observations at 300-s resolution had MVD values that exceeded the FAR 25-C envelopes. Regardless of the classification scheme, it is clear from the CFDE data that hazardous icing conditions associated with SLD were frequent enough that they should be considered by the aviation regulatory authorities.
- 5) Mixed-phase conditions with ice-crystal concentrations greater than  $5 \text{ L}^{-1}$  accounted for 11% of the icing environments measured, and mixed-phase conditions with ice-crystal concentrations between 1 and  $5 \text{ L}^{-1}$  accounted for an additional 11%. A significant portion of icing environments clearly are of mixed phase. Ice crystals dominate the FSSP measurements for sizes greater than  $35 \mu\text{m}$ , whereas misinterpretation of crystals as drops can be significant for 2D-C measurements for sizes less than or equal to 8 pixels ( $200 \mu\text{m}$ ). Therefore, for mixed-phase conditions with ice-crystal concentrations greater than  $1 \text{ L}^{-1}$  it is not feasible to measure the icing environment between approximately 35 and  $200 \mu\text{m}$  using FSSP and 2D-C probes. Assessing the icing environments associated with mixed-phase conditions, as outlined by Riley (1998) or as discussed in the FAA Inflight Aircraft Icing Plan, will require different instrumentation.
- 6) The 30-, 60-, 120-, and 300-s data were averaged into the size bins proposed by Jeck (1996). There was a 25% difference between the average LWC values for the 30-s (3 km) and 300-s (30 km) data, which demonstrated that the clouds measured were relatively uniform over a large horizontal extent. The 99.5th-percentile values were determined for each averaging interval and are representative of the extreme values observed during the two CFDE projects. Considerable additional data will need to be

collected before the 99.9th-percentile values can be assessed.

*Acknowledgments.* Funding for this research was provided by the Canadian National Search and Rescue Secretariat, Environment Canada, the National Research Council of Canada, Transport Canada, and Boeing Commercial Airplane Group. The authors acknowledge all the MSC and NRC participants of the CFDE field projects for their dedication toward obtaining a valuable dataset. The NRC pilots are thanked for their safe and efficient operations of the Convair-580. The authors thank A. Korolev for his helpful comments during the course of the field projects and postproject analysis and acknowledge D. Marcotte for his significant contributions in planning and conducting the CFDE projects.

#### REFERENCES

- Ashenden, R., and J. D. Marwitz, 1998: Characterizing the supercooled large droplet environment with corresponding turboprop aircraft response. *J. Aircraft*, **35**, 912–920.
- , W. Lindberg, J. D. Marwitz, and B. Hoxie, 1996: Aerofoil performance degradation by supercooled cloud, drizzle and rain drop icing. *J. Aircraft*, **33**, 1040–1046.
- Baumgardner, D., 1983: An analysis and comparison of five water droplet measuring instruments. *J. Climate Appl. Meteor.*, **22**, 891–910.
- , and A. Rodi, 1989: Laboratory and wind tunnel evaluations of the Rosemount icing detector. *J. Atmos. Oceanic Technol.*, **6**, 971–979.
- Beard, K. V., and H. T. Ochs, 1993: Warm-rain initiation: An overview of microphysical mechanisms. *J. Appl. Meteor.*, **32**, 608–625.
- Bernstein, B. C., T. P. Ratvasky, D. R. Miller, and F. McDonough, 1999: Freezing rain as an in-flight hazard. Preprints, *Eighth Conf. on Aviation, Range, and Aerospace Meteor.*, Dallas, TX, Amer. Meteor. Soc., 38–42.
- Biter, C. J., J. E. Dye, D. Huffman, and W. D. King, 1987: The drop-size response of the CSIRO liquid water probe. *J. Atmos. Oceanic Technol.*, **4**, 359–367.
- Bocchieri, J. R., 1980: The objective use of upper air soundings to specify precipitation type. *Mon. Wea. Rev.*, **108**, 596–603.
- Boutanios, Z., Y. Bourgault, W. G. Habashi, G. A. Isaac, and S. G. Cober, 1998: 3D droplets impingement analysis around an aircraft's nose and cockpit using FENSAP-ICE. *36th AIAA Aerospace Sciences Meeting and Exhibit*, Reno, NV, AIAA, Paper 98-0200.
- Cober, S. G., G. A. Isaac, and J. W. Strapp, 1995: Aircraft icing measurements in east coast winter storms. *J. Appl. Meteor.*, **34**, 88–100.
- , J. W. Strapp, and G. A. Isaac, 1996: An example of supercooled drizzle drops formed through a collision-coalescence process. *J. Appl. Meteor.*, **35**, 2250–2260.
- , G. A. Isaac, A. V. Korolev, and J. W. Strapp, 2001a: Assessing cloud-phase conditions. *J. Appl. Meteor.*, **40**, 1967–1983.
- , —, and —, 2001b: Assessing the Rosemount icing detector with in-situ measurements. *J. Atmos. Oceanic Technol.*, **18**, 515–528.
- Cooper, W. A., W. R. Sand, M. K. Politovich, and D. L. Veal, 1984: Effects of icing on performance of a research aircraft. *J. Aircraft*, **21**, 708–715.
- Federal Aviation Administration, 1999: Appendix C. Airworthiness standard: Transport category airplanes, Part 25, Aeronautics and Space, Vol. 14, U.S. Code of Regulations, Office of the Federal Register, National Archives and Records Administration. [Avail-

- able from Superintendent of Documents, U.S. Government Printing Office, Washington, DC 20402-9328.
- Fuchs, W., and K.-P. Schickel, 1995: Aircraft icing in visual meteorological conditions below stratus clouds. *Atmos. Res.*, **36**, 339–345.
- Gardiner, B. A., and J. Hallett, 1985: Degradation of in-cloud forward scattering spectrometer probe measurements in the presence of ice particles. *J. Atmos. Oceanic Technol.*, **2**, 171–180.
- Hallett, J., and S. C. Mossop, 1974: Production of secondary ice particles during the riming process. *Nature*, **249**, 26–28.
- Heymsfield, A. J., and J. L. Parrish, 1978: A computational technique for increasing the effective sampling volume of the PMS two-dimensional particle size spectrometer. *J. Appl. Meteor.*, **17**, 1566–1572.
- Hobbs, P. V., and A. L. Rangno, 1996: Precipitation from a maritime cloud layer with very low droplet concentrations. *Atmos. Res.*, **40**, 99–107.
- Huffman, G. J., and G. A. Norman, 1988: The supercooled warm rain process and the specification of freezing precipitation. *Mon. Wea. Rev.*, **116**, 2172–2182.
- Isaac, G. A., S. G. Cober, A. V. Korolev, J. W. Strapp, A. Tremblay, and D. L. Marcotte, 1998: Overview of the Canadian Freezing Drizzle Experiment I, II, and III. Preprints, *Conf. on Cloud Physics*, Everett, WA., Amer. Meteor. Soc., 447–450.
- Jeck, R. K., 1996: Representative values of icing-related variables aloft in freezing rain and freezing drizzle. U.S. Department of Transportation Rep. DOT/FAA/AR-TN95/119, 44 pp.
- Joe, P., and R. List, 1987: Testing and performance of two-dimensional optical array spectrometers with greyscale. *J. Atmos. Oceanic Technol.*, **4**, 139–150.
- Jones, A. R., and W. Lewis, 1949: Recommended values of meteorological factors to be considered in the design of aircraft ice-prevention equipment. National Advisory Committee for Aeronautics Tech. Note 1855, 14 pp.
- Kajikawa, M., K. Kikuchi, Y. Asuma, Y. Inoue, and N. Sato, 2000: Supercooled drizzle formed by condensation-coalescence in the mid-winter season of the Canadian Arctic. *Atmos. Res.*, **52**, 293–301.
- King, W. D., D. A. Parkin, and R. J. Handsworth, 1978: A hot wire liquid water device having fully calculable response characteristics. *J. Appl. Meteor.*, **17**, 1809–1813.
- , J. E. Dye, J. W. Strapp, D. Baumgardner, and D. Huffman, 1985: Icing wind tunnel tests on the CSIRO liquid water probe. *J. Atmos. Oceanic Technol.*, **2**, 340–352.
- Korolev, A. V., and G. A. Isaac, 2000: Drop growth due to high supersaturation caused by isobaric mixing. *J. Atmos. Sci.*, **57**, 1675–1685.
- , S. V. Kuznetsov, Y. E. Makarov, and V. S. Novikov, 1991: Evaluation of measurements of particle size and sample area from optical array probes. *J. Atmos. Oceanic Technol.*, **8**, 514–522.
- , J. W. Strapp, and G. A. Isaac, 1998a: Evaluation of the accuracy of PMS optical array probes. *J. Atmos. Oceanic Technol.*, **15**, 708–720.
- , —, —, and A. N. Nevzorov, 1998b: The Nevzorov airborne hot-wire LWC–TWC probe: Principles of operation and performance characteristics. *J. Atmos. Oceanic Technol.*, **15**, 1495–1510.
- Lewis, W., 1951: Meteorological aspects of aircraft icing. *Compendium of Meteorology*, T. F. Malone, Ed., Amer. Meteor. Soc., 1197–1203.
- , and N. R. Bergeron, 1952: A probability analysis of the meteorological factors conducive to aircraft icing in the United States. NACA Tech. Note 2738, 93 pp.
- Ludlam, F. H., 1951: The heat economy of a rimed cylinder. *Quart. J. Roy. Meteor. Soc.*, **77**, 663–666.
- Marwitz, J., M. Politovich, B. Bernstein, F. Ralph, P. Neiman, R. Ashenden, and J. Bresch, 1997: Meteorological conditions associated with the ATR72 aircraft accident near Roselawn, Indiana, on 31 October 1994. *Bull. Amer. Meteor. Soc.*, **78**, 41–52.
- McKay, G. A., and H. A. Thompson, 1969: Estimating the hazard of ice accretion in Canada from climatological data. *J. Appl. Meteor.*, **8**, 927–935.
- Miller, D., T. Ratvasky, B. Bernstein, F. McDonough, and J. W. Strapp, 1998: NASA/FAA/NCAR supercooled large droplet icing flight research: Summary of winter 96–97 flight operations. *36th AIAA Aerospace Sciences Meeting and Exhibit*, Reno, NV, AIAA, Paper 98-0577.
- Miller, D. R., H. E. Addy, and R. F. Ide, 1996: A study of large droplet ice accretions in the NASA-Lewis IRT at near-freezing conditions. *34th AIAA Aerospace Sciences Meeting and Exhibit*, Reno, NV, AIAA Paper 96-0934.
- Newton, D. W., 1978: An integrated approach to the problem of aircraft icing. *J. Aircraft*, **15**, 374–380.
- Pobanz, B. M., J. D. Marwitz, and M. K. Politovich, 1994: Conditions associated with large-drop regions. *J. Appl. Meteor.*, **33**, 1366–1372.
- Politovich, M. K., 1989: Aircraft icing caused by large supercooled droplets. *J. Appl. Meteor.*, **28**, 856–868.
- , 1996: Response of a research aircraft to icing and evaluation of severity indices. *J. Aircraft*, **33**, 291–297.
- Pruppacher, H. R., and J. D. Klett, 1978: *Microphysics of Clouds and Precipitation*. D. Reidel, 714 pp.
- Reisner, J., R. M. Rasmussen, and R. T. Bruintjes, 1998: Explicit forecasting of supercooled liquid water in winter storms using the MM5 mesoscale model. *Quart. J. Roy. Meteor. Soc.*, **124**, 1071–1107.
- Riley, R. K., 1998: Mixed-phase icing conditions: A review. U.S. Dept. of Transportation Rep. DOT/FAA/AR-98/76, 45 pp.
- Sand, W. R., W. A. Cooper, M. K. Politovich, and D. L. Veal, 1984: Icing conditions encountered by a research aircraft. *J. Climate Appl. Meteor.*, **23**, 1427–1440.
- Singleton, F., 1960: Aircraft observations of rain and drizzle from layer clouds. *Quart. J. Roy. Meteor. Soc.*, **86**, 195–204.
- Stewart, R. E., 1991: Canadian Atlantic Storms Program: Progress and plans of the meteorological component. *Bull. Amer. Meteor. Soc.*, **72**, 364–371.
- , 1992: Precipitation types in the transition region of winter storms. *Bull. Amer. Meteor. Soc.*, **73**, 287–296.
- , and R. W. Crawford, 1995: Some characteristics of the precipitation formed within winter storms over eastern Newfoundland. *Atmos. Res.*, **36**, 17–37.
- Strapp, J. W., R. A. Stuart, and G. A. Isaac, 1996: A Canadian climatology of freezing precipitation, and a detailed study using data from St. John's, Newfoundland. *Proc. Int. Conf. on Aircraft Inflight Icing*, Springfield, VA, Federal Aviation Administration, 45–56.
- , J. Oldenburg, R. Ide, Z. Vukovic, S. Bacic, and L. Lilie, 2000: Measurements of the response of hot wire LWC and TWC probes to large droplet clouds. *Proc. 13th Int. Conf. on Clouds and Precipitation*, Reno, NV, 181–184.
- , F. Albers, A. Reuter, A. V. Korolev, W. Maixner, E. Rashke, and Z. Vukovic, 2001: Laboratory measurements of the response of a PMS OAP-2DC probe. *J. Atmos. Oceanic Technol.*, **18**, 1150–1170.
- Stuart, R. A., and G. A. Isaac, 1999: Freezing precipitation in Canada. *Atmos.–Ocean*, **37**, 87–102.
- Tremblay, A., and A. Glazer, 2000: An improved modeling scheme for freezing precipitation forecasts. *Mon. Wea. Rev.*, **128**, 1289–1308.
- Zerr, R. J., 1997: Freezing rain: An observational and theoretical study. *J. Appl. Meteor.*, **36**, 1647–1661.